III

ELASTIC PROPERTIES AND POROSITY

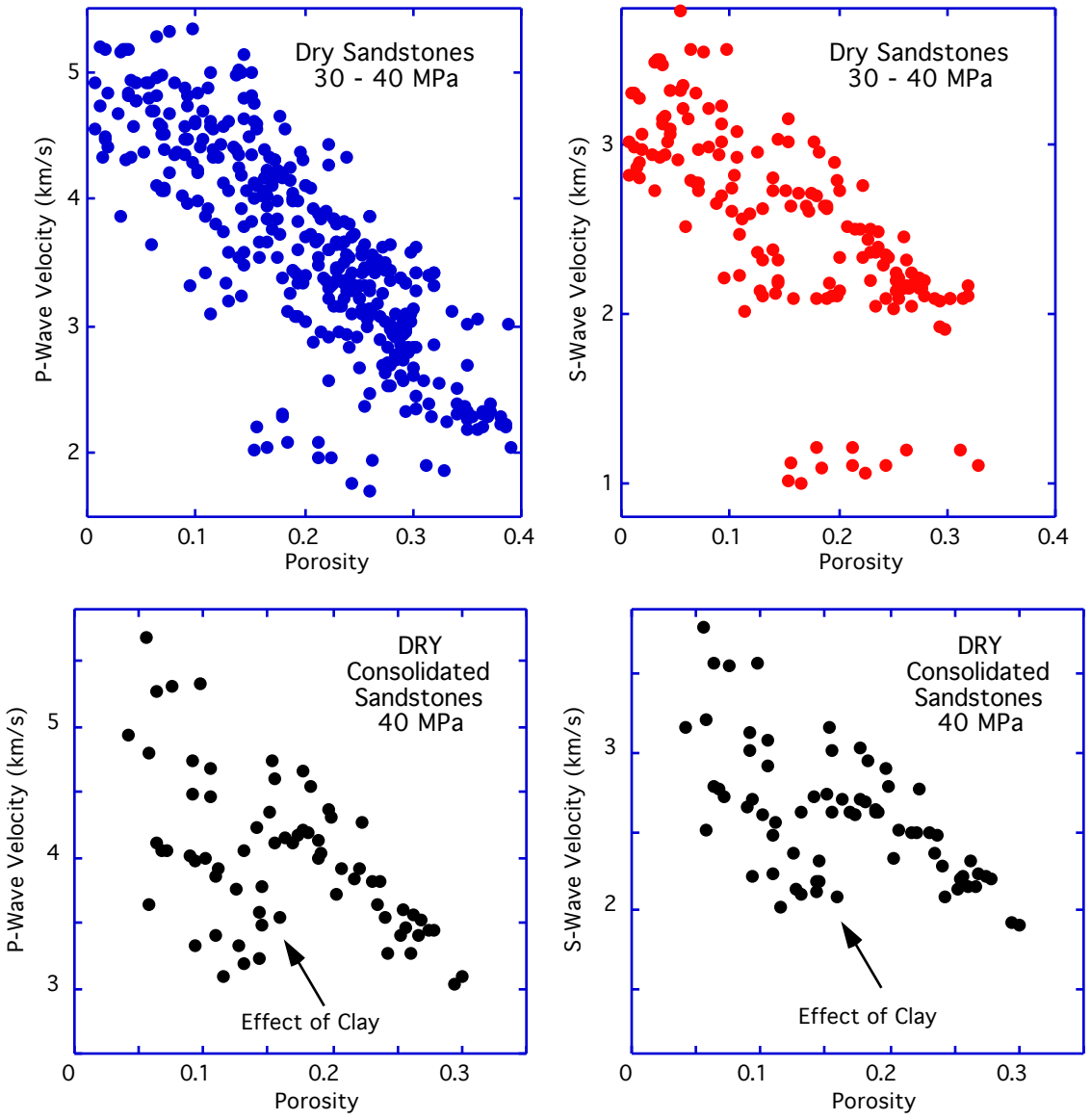

Diversity in high-porosity sandstones.

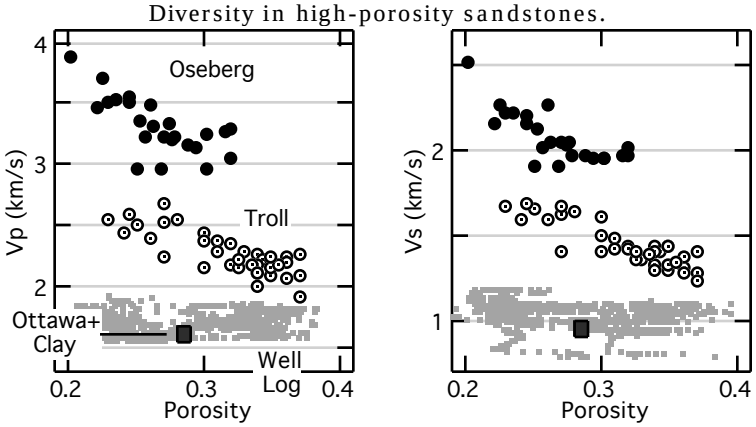

2. Critical Porosity Concept

Many natural and artificial rocks have a porosity limit above which they can exist only as suspensions. This limit -- the critical porosity -- is closely linked to the formation process and micro-topology inherent to a class of rocks. For example, in sandstones, the critical porosity is 36% - 40% -- the porosity of a random close pack of well-sorted rounded quartz grains. This pack is often the starting point for the formation of consolidated sandstones. On the other hand, in natural and artificial foams (pumice, glass foam), the critical porosity is higher than 90%. The honeycomb micro-topology of foams allows the material to stay intact up to a very high porosity. Similar considerations are true for other rocks, such as dolomites, carbonates, chalks, and cracked igneous rocks. The critical porosity separates two principal domains in the porosity range: rock is in the consolidated, frame-supporting state in the domain from zero to the critical porosity, and is in the suspension, fluid-supporting state in the domain from the critical porosity to 100%. This critical porosity principle allows one to revisit and improve the traditional effective medium theories where a single model attempts to relate the elastic and other properties of rocks to porosity in the whole porosity range -- from zero to 100%. Now, by separating this range into the above two domains, it is possible to use more physical, and accurate, effective medium models in each domain.

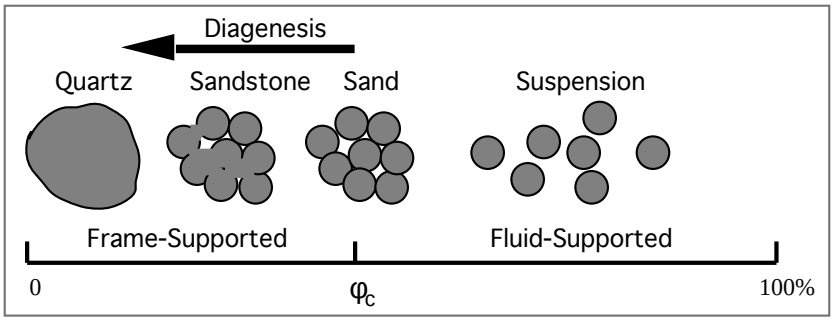

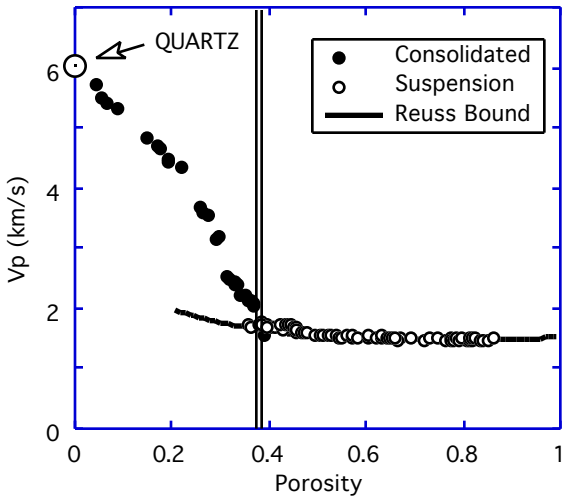

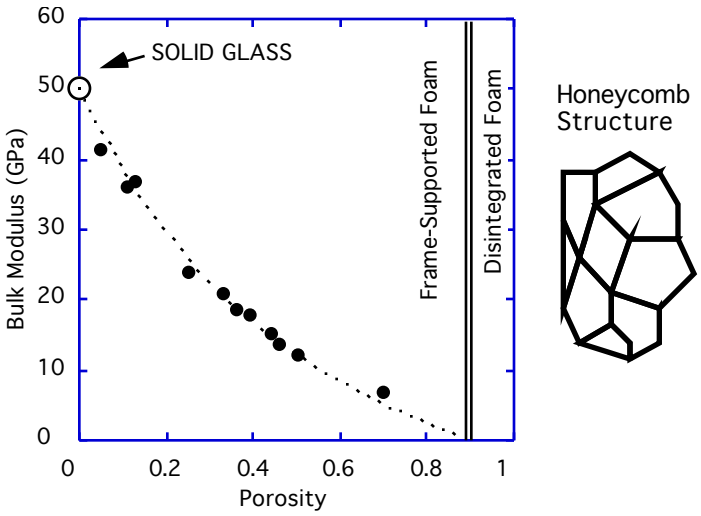

A *critical porosity* value exists which is typical for a given class of porous materials. Each class is defined on the basis of common mineralogy and/or diagenetic porosity reduction process. In order to validate this hypothesis and support the above-formulated critical porosity concept, we present data collected by various authors for different rock types.

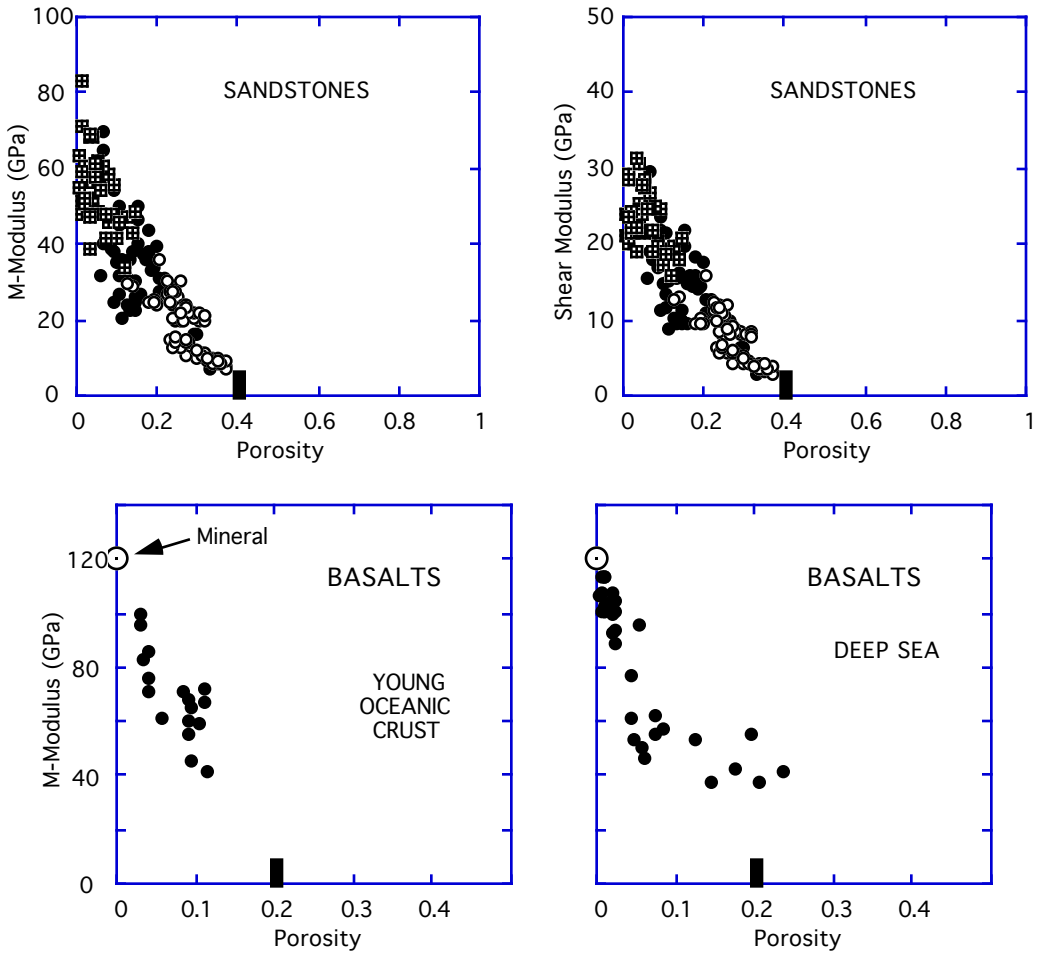

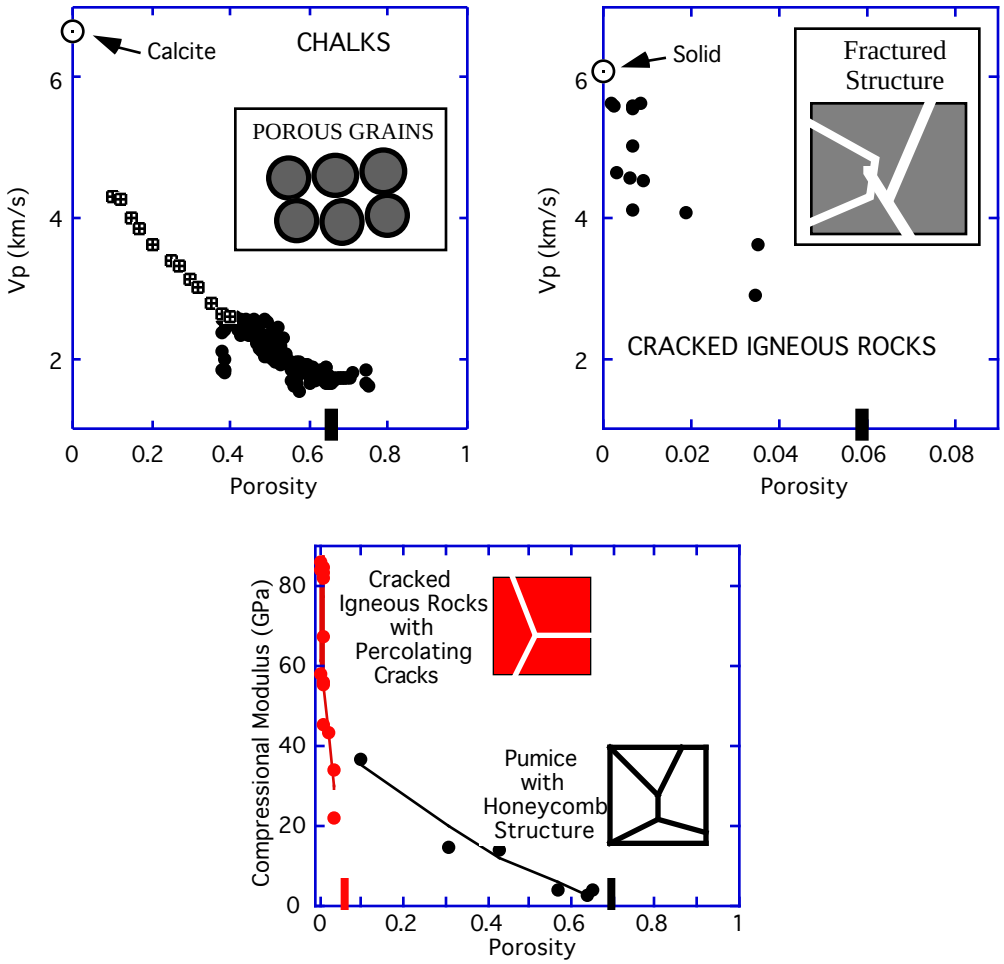

Material	Critical Porosity
Sandstones	40%
Limestones	40%
Dolomites	40%
Pumice	80%
Chalks	65%
Rock Salt	40%
Cracked Igneous Rocks	5%
Oceanic Basalts	20%
Sintered Glass Beads	40%
Glass Foam	90%

3. Critical Concentration Concept

The critical porosity concept leads to the "critical concentration" concept used to describe the properties of sands with shale. Consider the experimental data from Yin (1993) obtained on samples hand-made by mixing Ottawa sand and kaolinite. The volumetric clay content in the samples varied from 0 to 100%.

The total porosity at 20 MPa differential pressure is plotted versus the volumetric clay content below. The two end members of the data set are the porosity of Ottawa sand at zero clay content and porosity of kaolinite at 100% clay content. The porosity of the mixture

reaches its minimum at the point where the volumetric concentration of clay equals the porosity of Ottawa sand which is closer to the critical porosity for sandstones. This clay content is called "critical clay concentration." The critical concentration is important not only for the total porosity but also for the elastic moduli of the mixture. The stiffness of the mixture is maximum at the critical concentration and decreases as the clay content increases or decreases from the critical concentration value. Poisson's ratio behaves in a similar way.

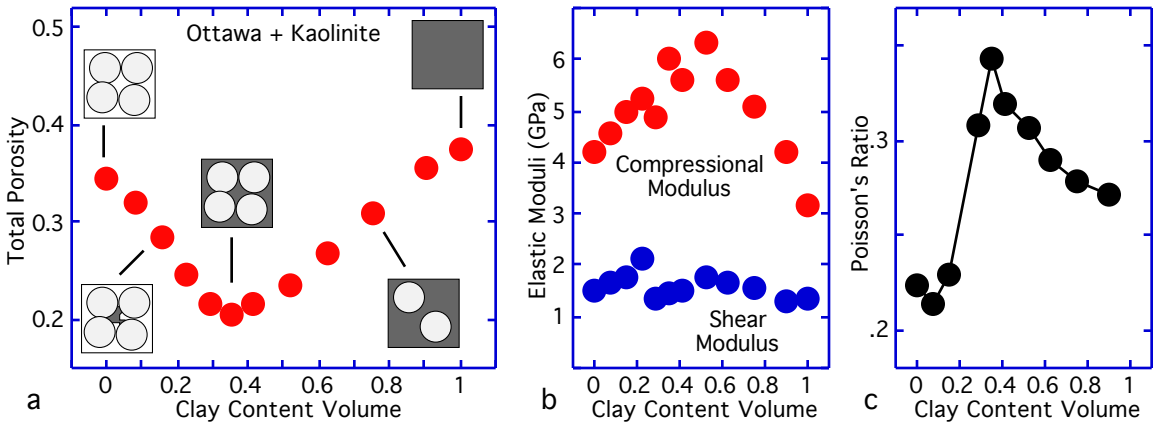

The elastic properties of the Ottawa sand and kaolinite mixture are plotted versus the total porosity below. The non-uniqueness of the elastic moduli, and, especially, Poisson's ratio in the cross-plots is due to the grain-scale texture of the rock.

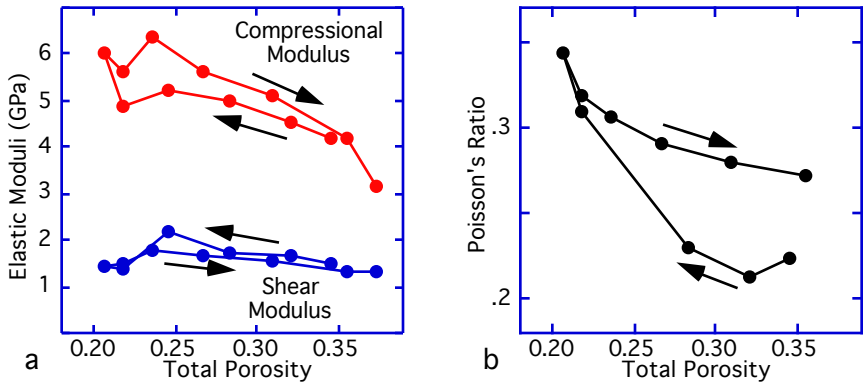

This effect has to be considered when examining well-log data. Below we plot the bulk density and P-wave impedance versus the gamma-ray values for a well in Colombia. The trends have the low-gamma-ray and the high-gamma-ray branches. This effect that is a result of the rock's microstructure results in non-uniqueness as the P-wave impedance is plotted versus the bulk density and porosity. Being aware of the physical reason underlying these non-unique cross-plots will allow the log analyst to separate the trends and arrive at accurate impedance-porosity transforms.

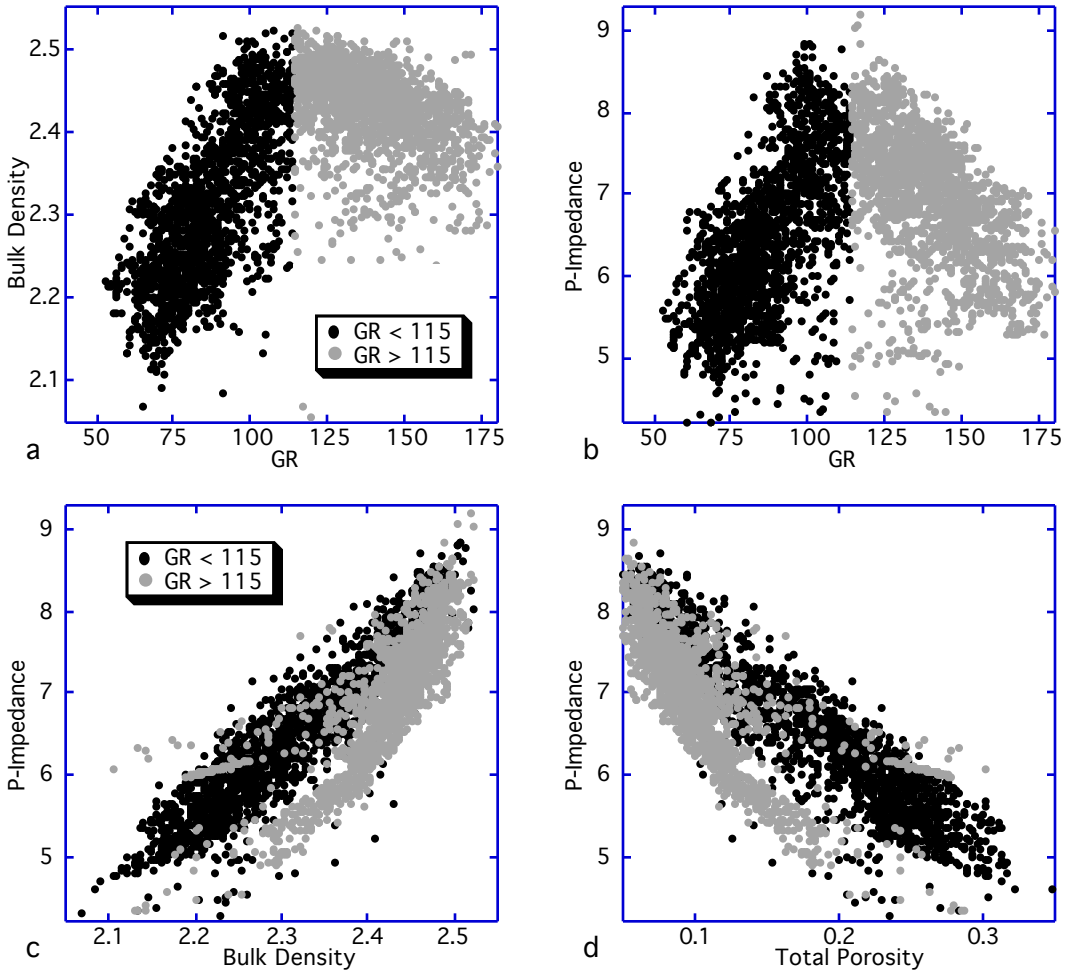

5. Role of Clay and La Cira Study

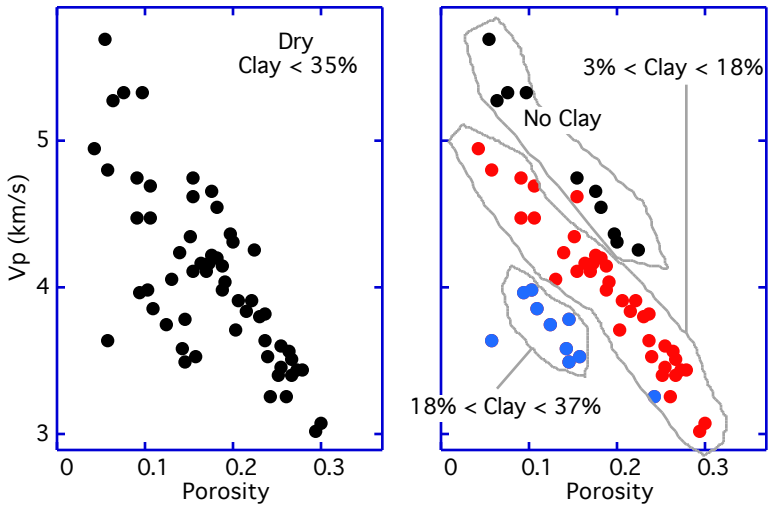

Clay tends to soften the rock frame. Han's (1986) equations are (velocity is in km/s):

$$V_p = 5.41 - 6.35\phi - 2.87C,\ V_s = 3.57 - 4.57\phi - 1.83C.$$

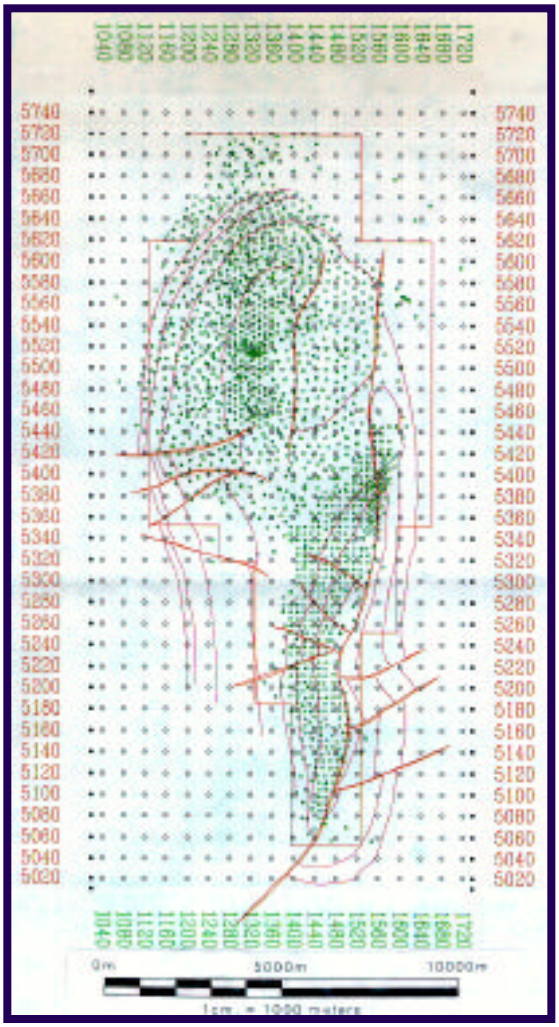

- **Discovered in 1918**
- **OOIP: 3490 MMBO**
- **1742 wells**
- **Production: 721 MMBO**
- **Recovery factor (20%)**

La Cira field has a very low recovery rate. The problem is highly heterogeneous depositional environment where thin sands are surrounded by shale layers.

The goal of the study is to map sands and shales from 3D seismic data.

Two typical vertical intervals from La Cira wells are shown below.

The low shale content typically corresponds to high oil saturation and ***high velocity***. The fact that shale has velocity higher than sand contradicts our earlier observations that clay tends to soften sandstone.

The cross-plots of velocity versus shale content and velocity versus porosity show that there is a clear trend of velocity increasing with the increasing shale content and with decreasing porosity.

The question is: Why does the velocity-porosity cross-plot show a uniform linear trend for both sands and shales?

Can this transform be used for interpreting seismic data?

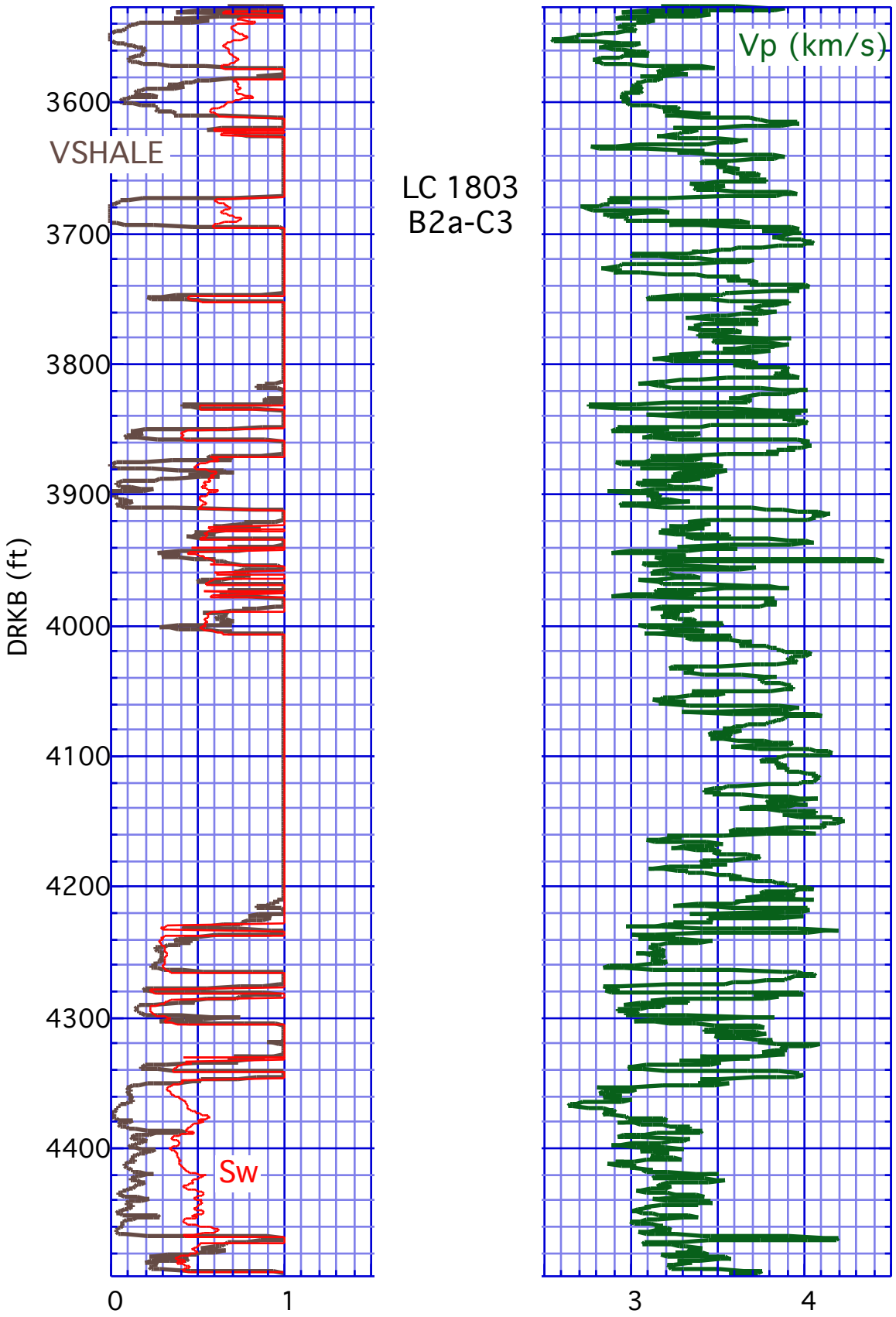
LC 1803
B2a-C3
VSHALE
Sw
Vp (km/s)
DRKB (ft)
3600
3700
3800
3900
4000
4100
4200
4300
4400
0
1
3
4

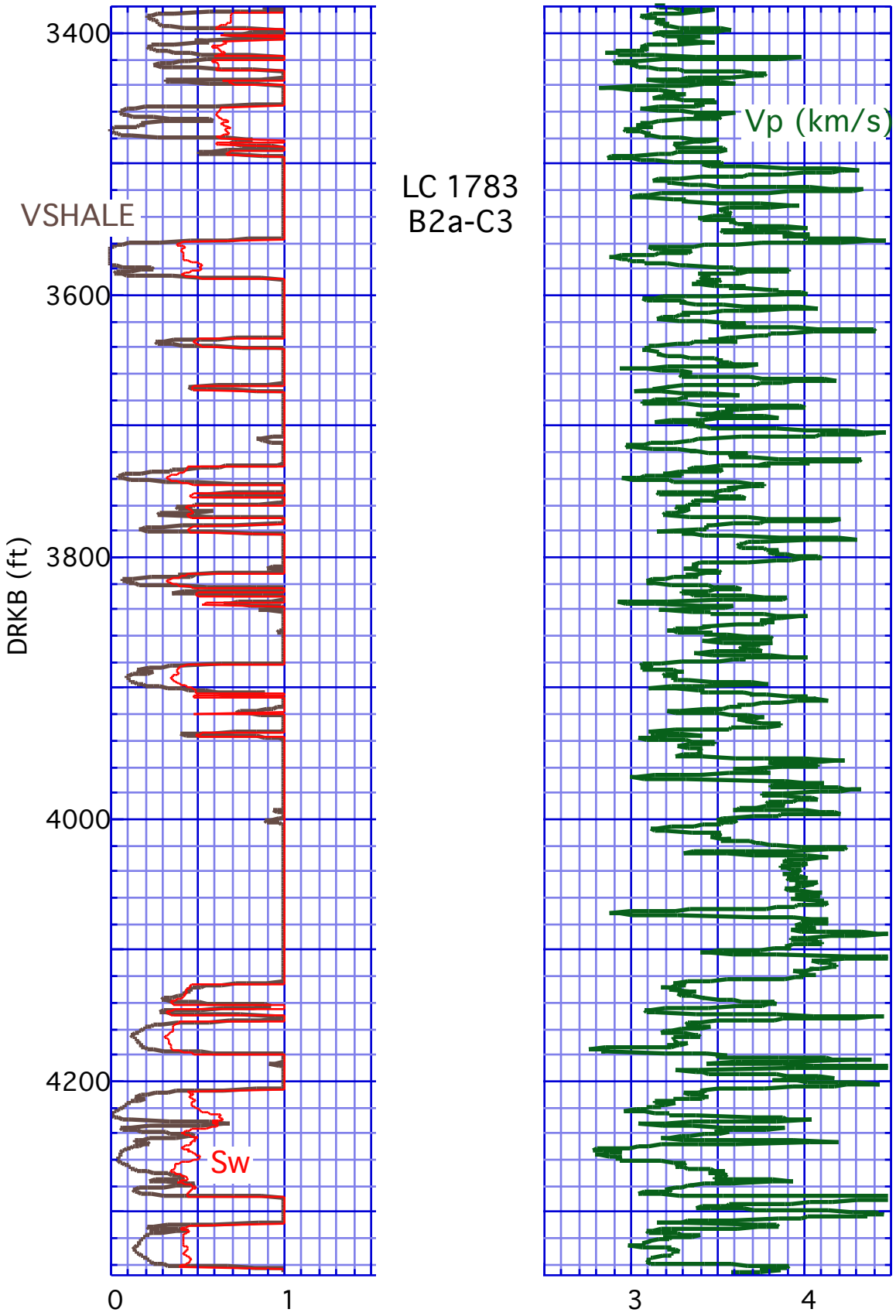
3400
3600
3800
4000
4200
DRKB (ft)
VSHALE
Sw
0
1
LC 1783
B2a-C3
Vp (km/s)
3
4

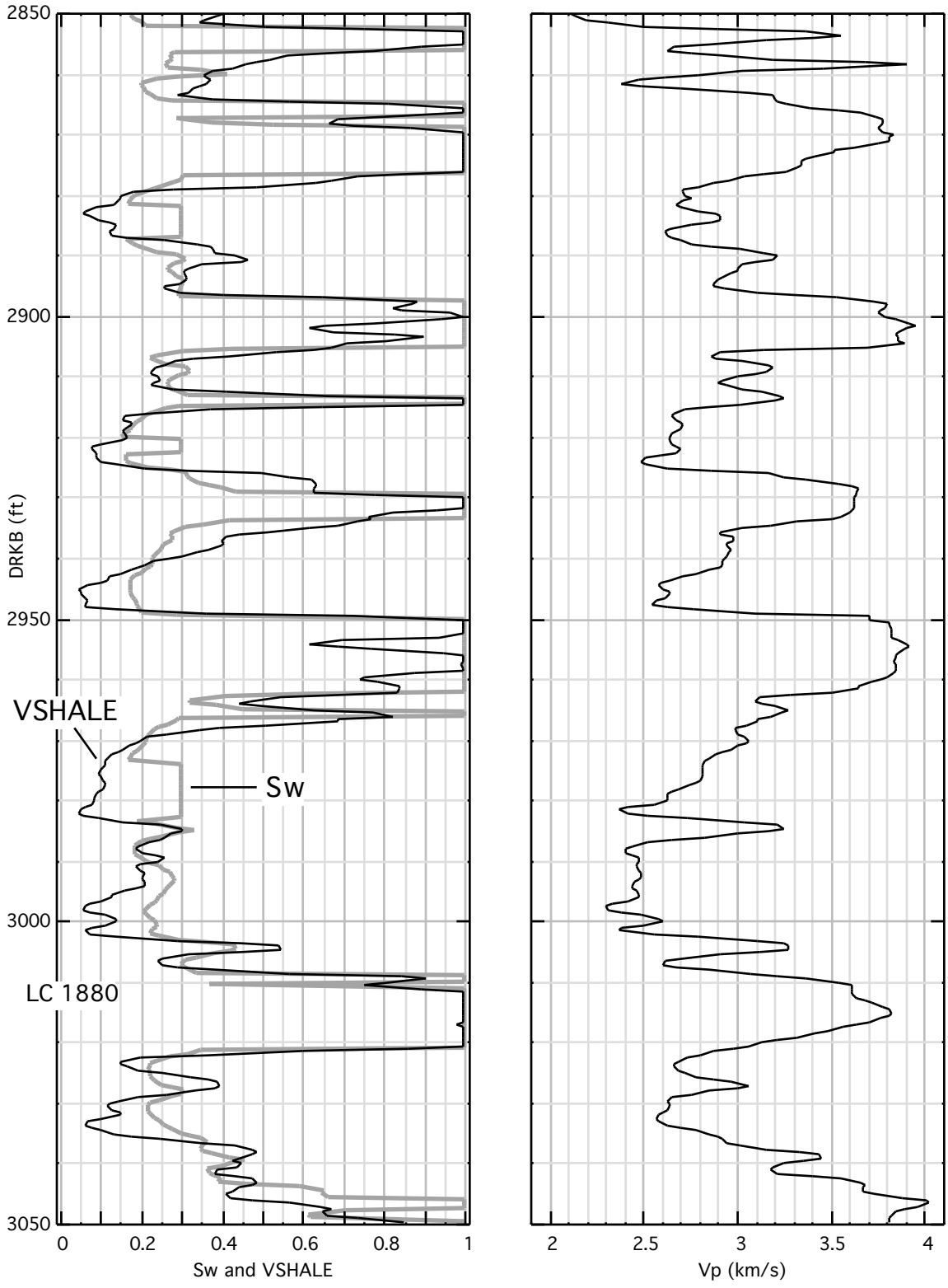
2850
2900
2950
3000
3050
DRKB (ft)
VSHALE
Sw
LC 1880
0
0.2
0.4
0.6
0.8
1
Sw and VSHALE
2
2.5
3
3.5
4
Vp (km/s)

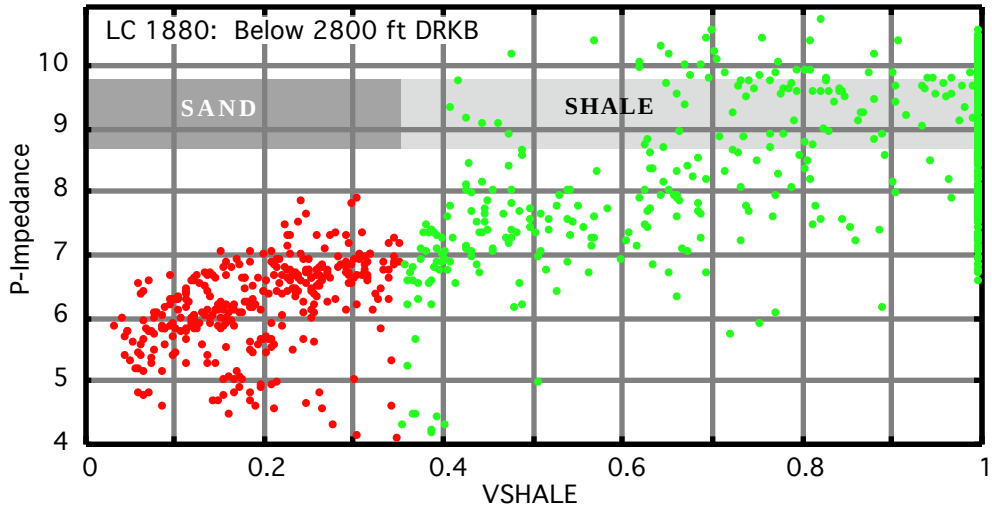

WHY VELOCITY IN SHALE IS LARGER THAN IN SAND -- POROSITY EFFECT?

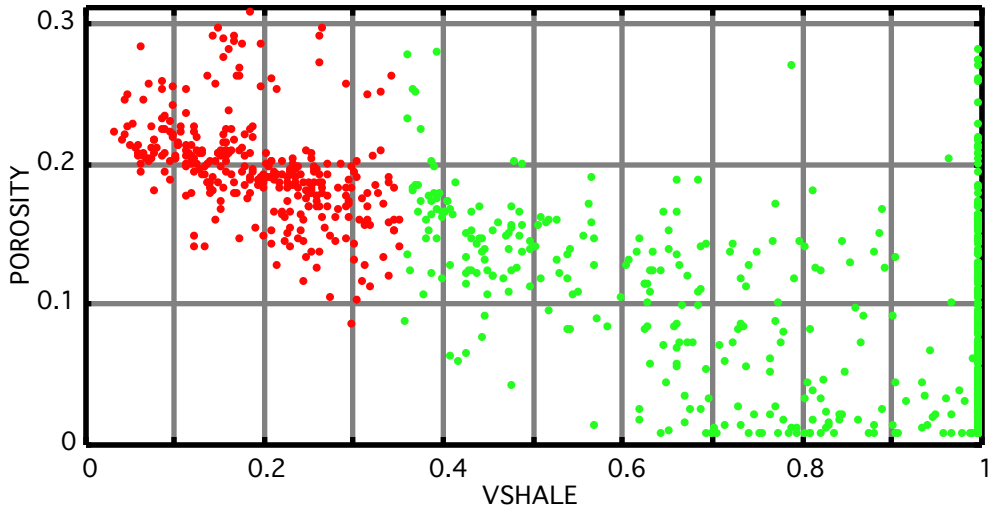

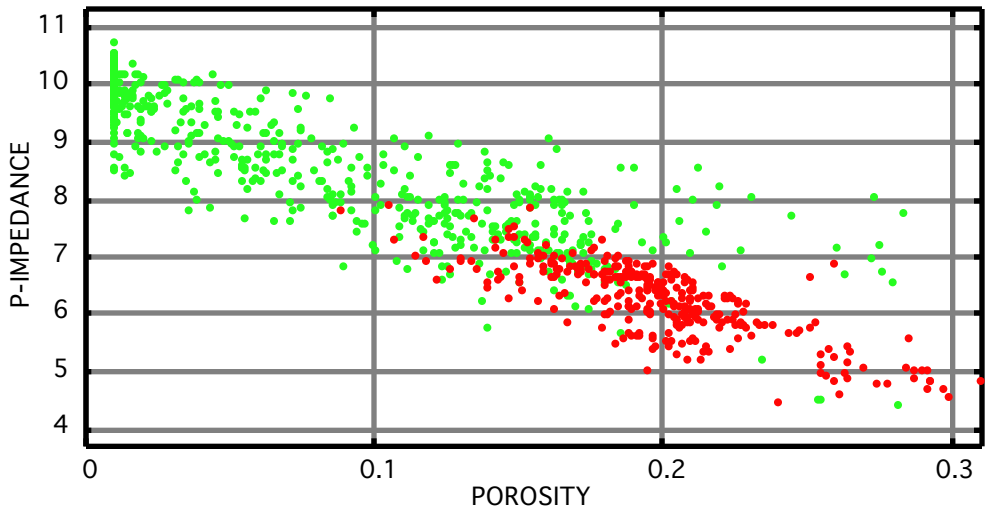

To answer these questions, we conduct laboratory measurements. We selected samples not only from the sandy zones but also from 100% shale zone to be able to understand the velocity behavior. The results show precisely the behavior observed in well logs: there is a uniform trend for sands and shales.

The most important insight comes from measuring mineralogical clay content using XRD. It appears that the actual clay content in the shale is not large. The shale is mostly siltstone rather than clay. Now the trend we see in the data is the velocity-porosity trend with almost uniform mineralogy.

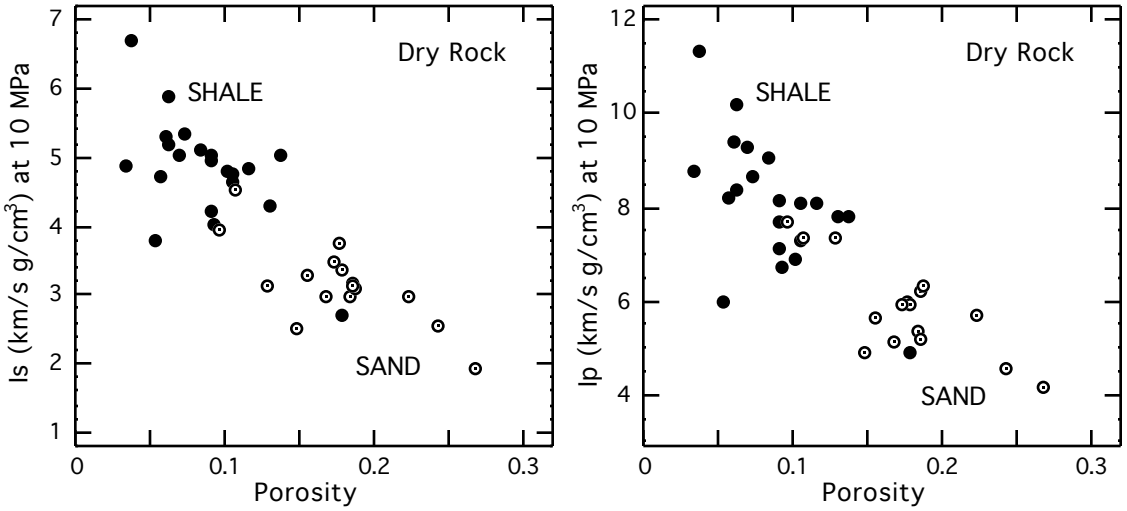

SAMPLES FROM SHALY ZONES

Sample ID	Porosity	Quartz	Clay	Feldspar	Calc+Dolom	Other
1880/2443'	0.033	0.610	0.290	0.080	0.000	0.020
1882/2743'	0.037	0.470	0.190	0.030	0.290	0.020
1879/1852'	0.054	0.720	0.260	0.010	0.000	0.010
1880/2452'	0.057	0.650	0.250	0.070	0.000	0.030
1882/2971'	0.061	0.560	0.240	0.110	0.050	0.040
1880/2457'10"	0.062	0.620	0.150	0.180	0.050	0.000
1880/2454'	0.062	0.660	0.240	0.060	0.020	0.020
1882/2612'	0.069	0.720	0.250	0.020	0.000	0.010
1880/2439'	0.073	0.680	0.220	0.090	0.000	0.010
1880/2417'	0.084	0.660	0.210	0.130	0.000	0.000
1879/1868'	0.091	0.650	0.320	0.020	0.000	0.010
1879/1923'	0.091	0.760	0.190	0.030	0.000	0.020
1879/1826'	0.092	0.770	0.150	0.060	0.000	0.020
1880/2432'4"	0.093	0.660	0.270	0.050	0.010	0.010
1879/1872'	0.103	0.660	0.180	0.140	0.000	0.020
1880/2399'	0.106	0.570	0.200	0.040	0.170	0.020
1879/1919'	0.106	0.830	0.150	0.010	0.000	0.010
1879/1871'	0.116	0.680	0.180	0.120	0.000	0.020
1879/1805'	0.131	0.680	0.110	0.210	0.000	0.000
1879/1877'	0.137	0.720	0.140	0.120	0.010	0.010
1879/1902'	0.178	0.820	0.100	0.080	0.000	0.000

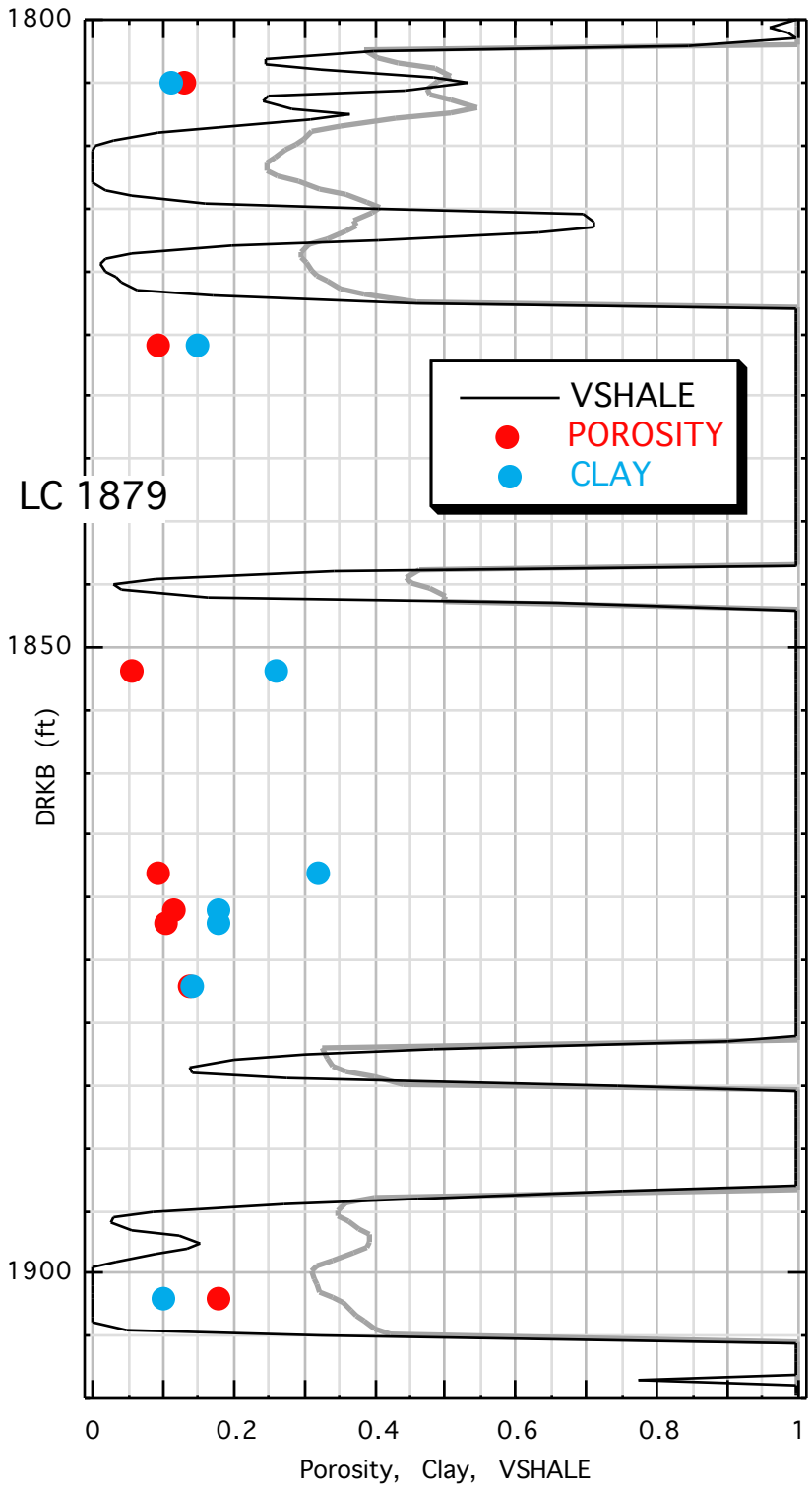

Next we use the seismic data to conduct impedance inversion. The impedance volumes can be directly interpreted as porosity volumes or shale content volumes.

We can clearly see sand channels and shale layers in the impedance images.

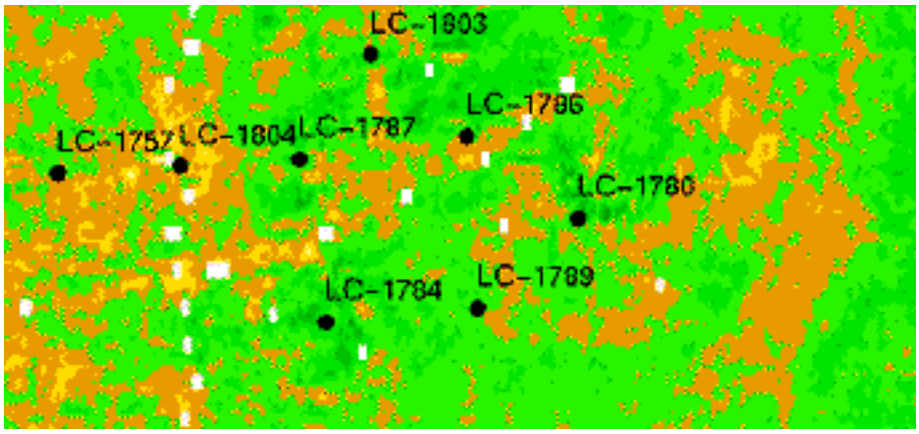

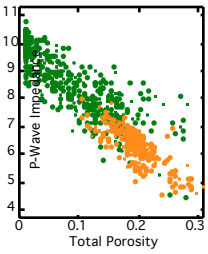

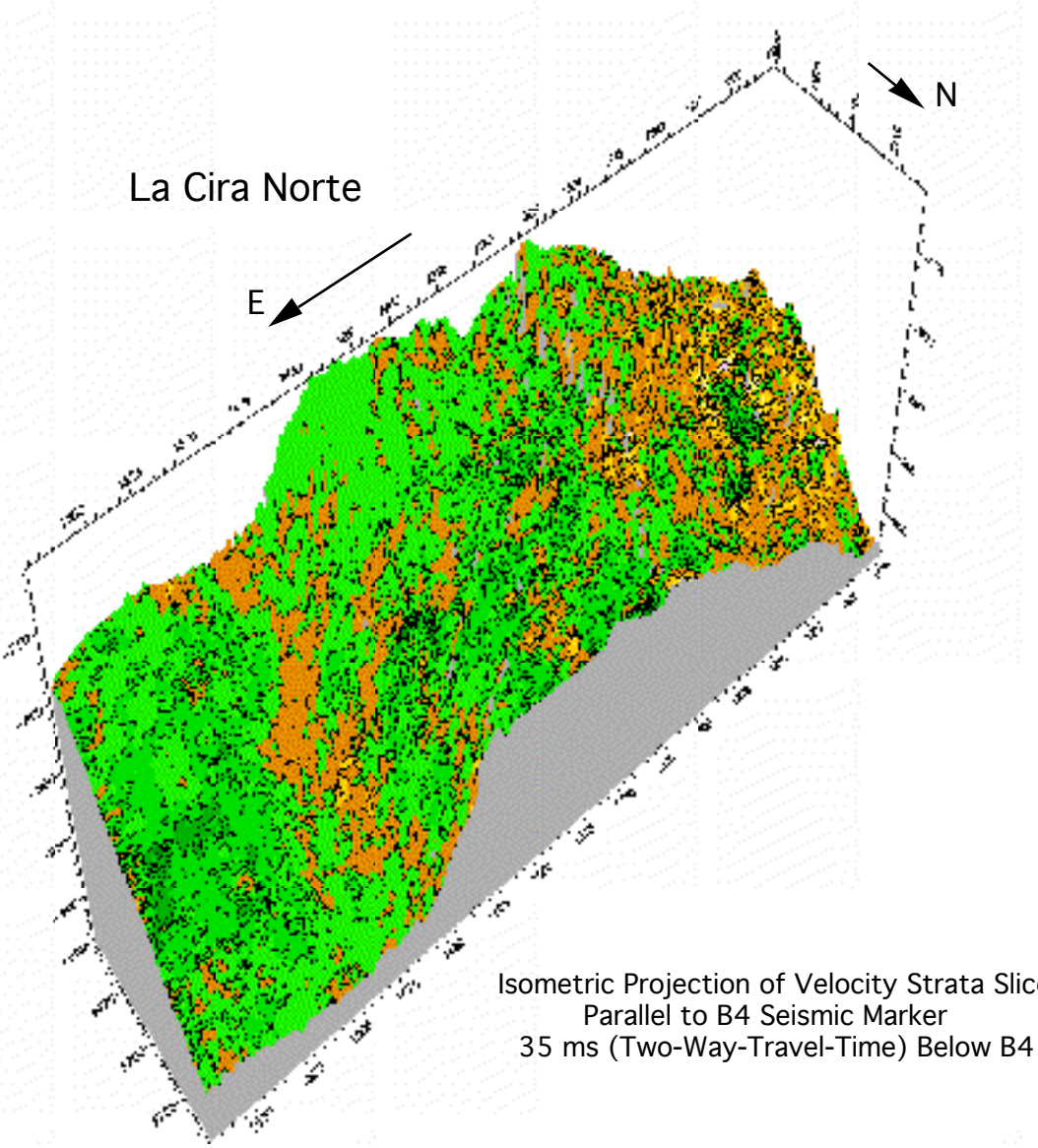

Isometric Projection of Velocity Strata Slice
Parallel to B4 Seismic Marker
35 ms (Two-Way-Travel-Time) Below B4

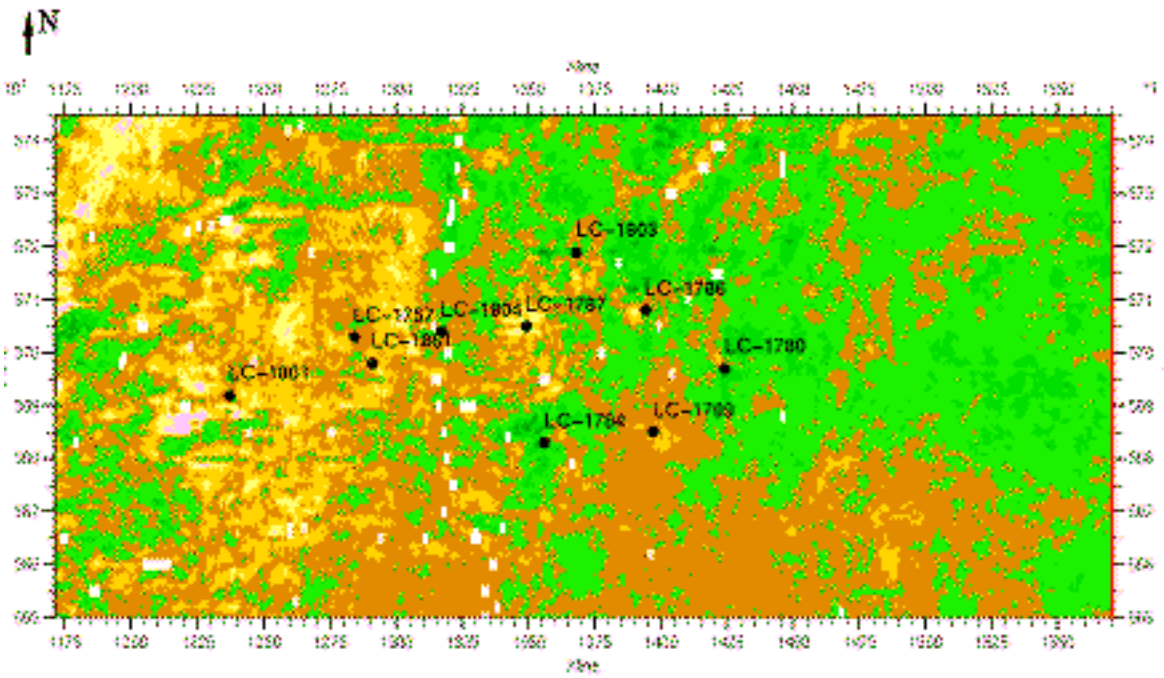
N
LC-1803
LC-1786
LC-1757
LC-1804
LC-1787
LC-1801
LC-1780
LC-1002
LC-1784
LC-1783

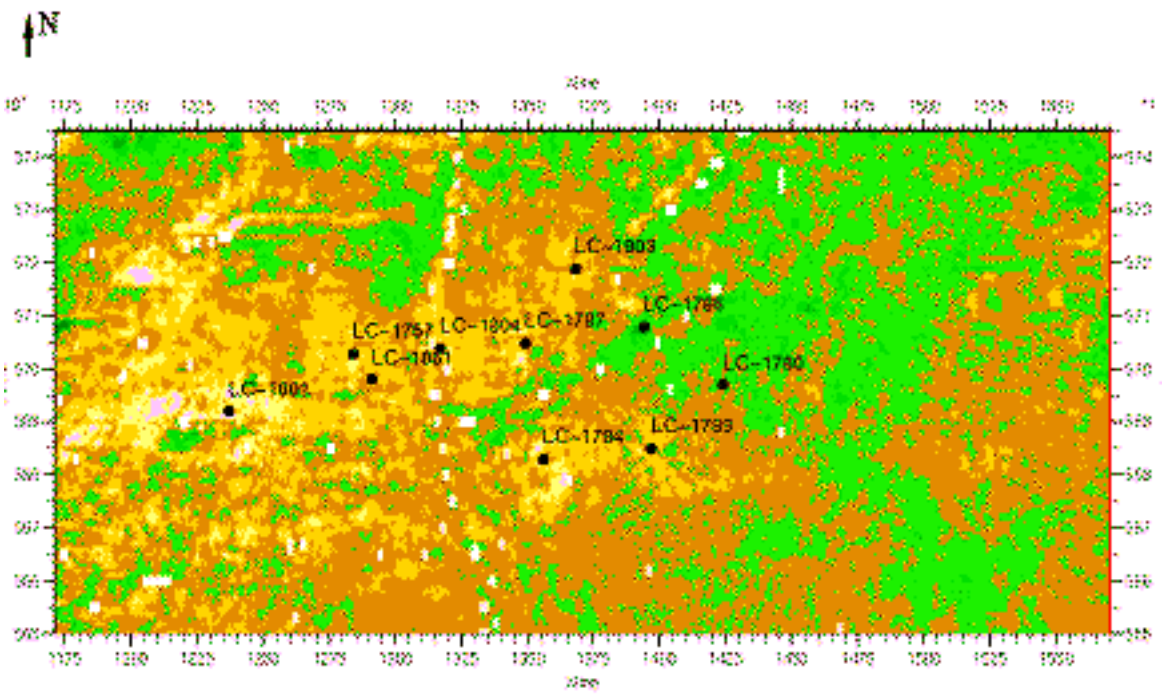
N
LC-1803
LC-1786
LC-1757
LC-1804
LC-1787
LC-1801
LC-1780
LC-1002
LC-1784
LC-1783

6. Commonly Used Velocity-Porosity Transforms

Expressions that relate velocity to porosity and to pore-fluid compressibility are among the most important deliverables of rock physics. Such relations are often used as additional controls for inferring porosity from well logs, as well as in-situ indicators of pore fluid type. The oldest and most popular is the Wyllie et al. (1956) equation:

$$\tau_P = \tau_S + \tau_F,$$

where τ_P is the measured travel time of a P-wave, τ_S is the travel time expected in the solid-phase material, and τ_F is that expected in the pore fluid. It follows from equation (1) that

$$\frac{1}{V_p} = \frac{1-\phi}{V_{pS}} + \frac{\phi}{V_{pF}},$$

where ϕ is porosity, V_p is the measured P-wave velocity, and V_{pS} and V_{pF} are the P-wave velocities in the solid and in the pore-fluid phases, respectively.

Wyllie's equation presents a simple and convenient, but deceptive form of summarizing extensive experimental data. Indeed, there is no physical reason for the total travel time of a wave in a two-component composite to be the sum of the travel times in the individual components (unless the two components are arranged in layers normal to the direction of propagation, and the wavelength is small as compared to the thickness of an individual layer).

Another simple velocity-porosity transform is that of Raymer. It is an empirical transform and Raymer (1980) does assign any physical meaning to it.

$$V_p = (1-\phi)^2 V_{pS} + \phi V_{pF}, \quad \phi < 0.37.$$

Is it necessary to abandon the non-physical time average equation, or equally simple traditional empirical relations, in favor of rigorous physics-oriented models?

Below, we plot velocity versus porosity for clean water-saturated fast and slow sandstones and superimpose the Wyllie and Raymer predictions.

Wyllie's equation underestimate the velocity while Raymer's equation predicts the velocity well for fast sandstones. ***These equations cannot be used for slow sands***.

Raymer's equation works well not only for clean sandstones but also for consolidated sandstones with clay (see below). We recommend using it for fast consolidated rocks.

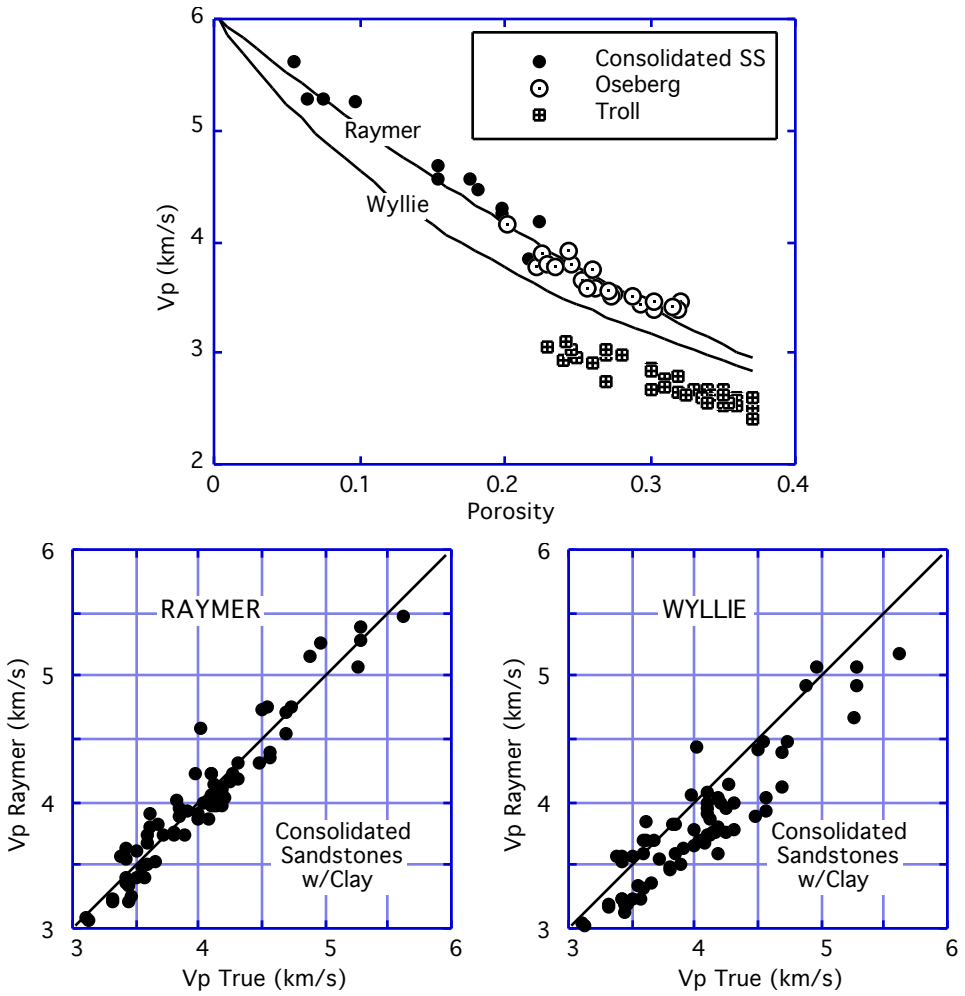

7. High-Porosity Sandstones

The situation is not that simple for high-porosity sandstones. Consider the plot below where clean sands have drastically different velocity in the same porosity range.

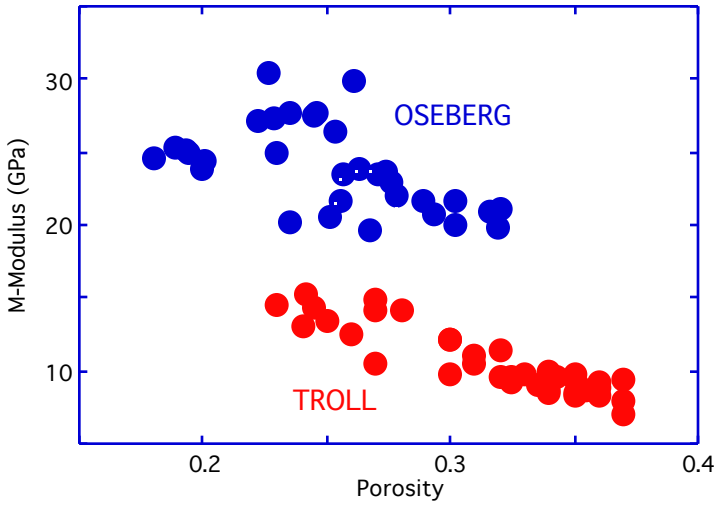

A way to understand this difference is to apply the critical porosity concept and hypothesize various velocity-porosity curves may propagate from the same staring point, depending on diagenesis.

This hypothesis is confirmed by the effective-medium modeling that shows clear separation between different diagenetic processes in the velocity-porosity plane.

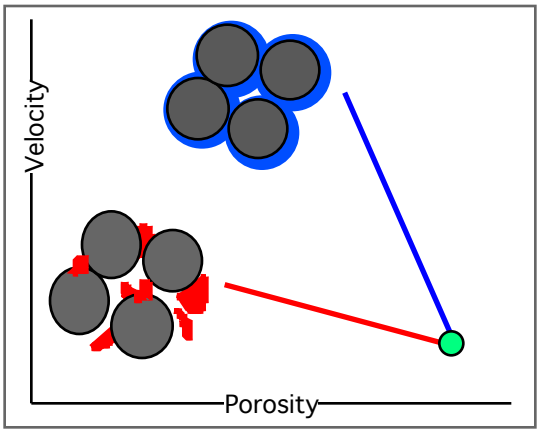

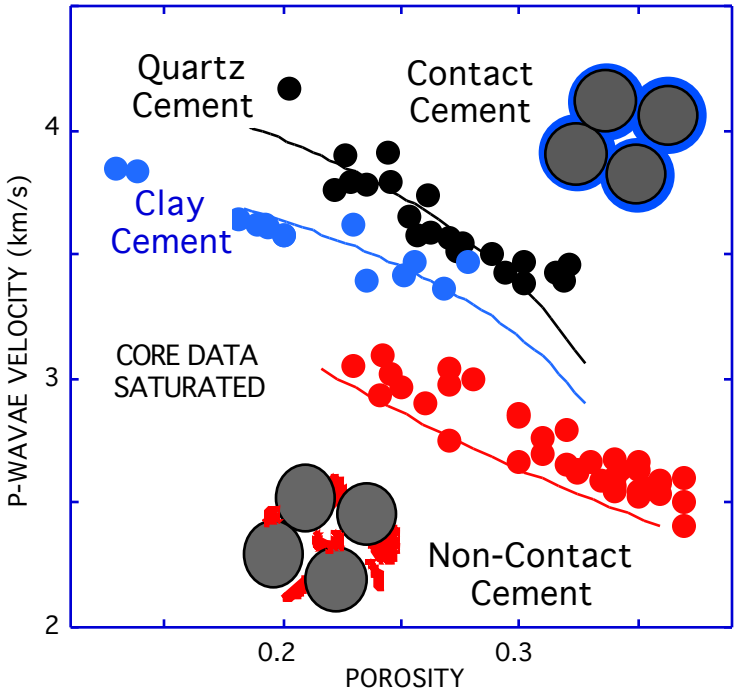

Such velocity-porosity patterns can be easily seen in well logs. It is important to discriminate between different patterns in order to property apply a velocity-porosity transform to seismic inversion data.

In the plots below we show a typical well log from a North Sea well where slightly cemented high-porosity sandstones are surrounded by unconsolidated shales.

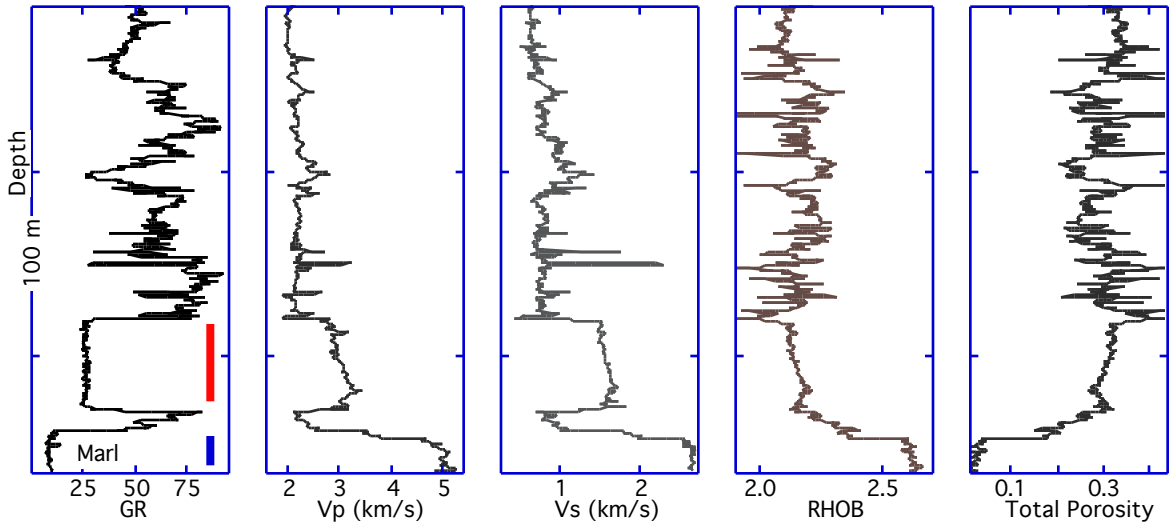
Depth
100 m
Marl
25 50 75
GR
2 3 4 5
Vp (km/s)
1 2
Vs (km/s)
2.0 2.5
RHOB
0.1 0.3
Total Porosity

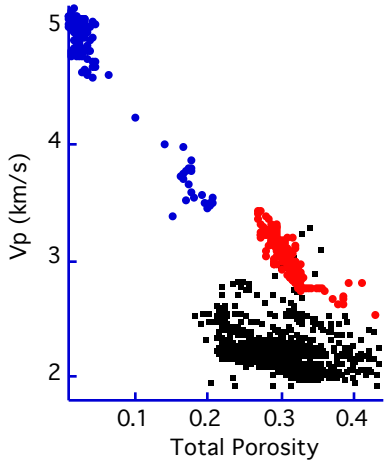
Vp (km/s)
5
4
3
2
0.1 0.2 0.3 0.4
Total Porosity

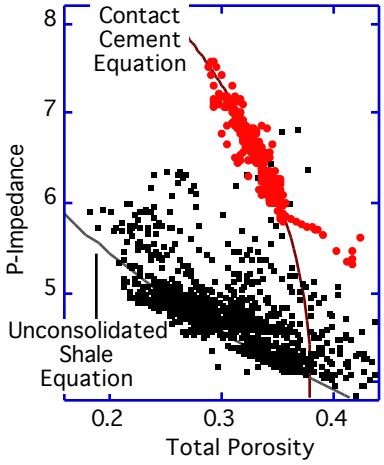
Contact
Cement
Equation
P-Impedance
8
7
6
5
Unconsolidated
Shale
Equation
0.2 0.3 0.4
Total Porosity

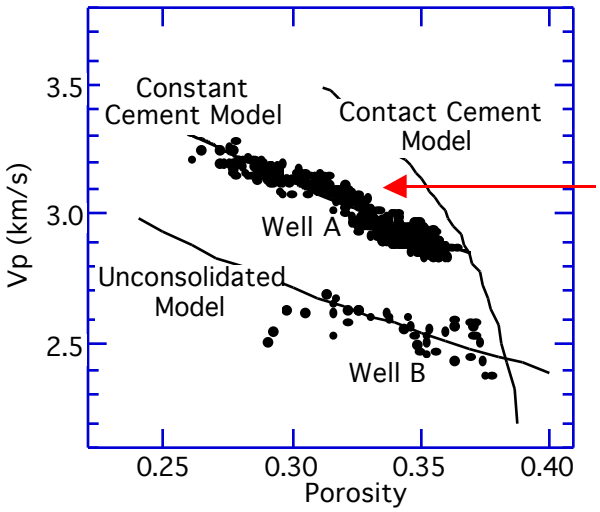
Constant
Cement Model
Contact Cement
Model
Well A
Unconsolidated
Model
Well B
Vp (km/s)
3.5
3.0
2.5
0.25 0.30 0.35 0.40
Porosity

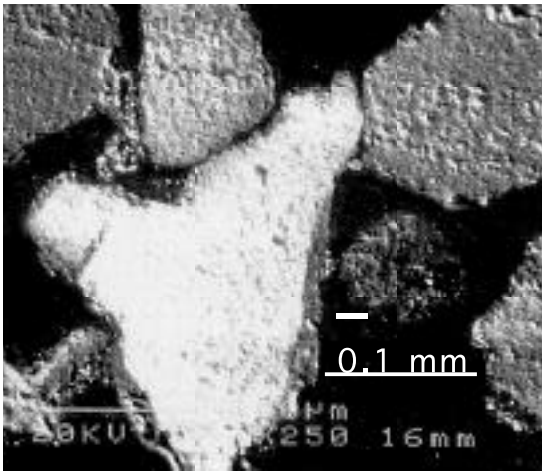
0.1 mm
16mm

8. CONTACT-CEMENT THEORY

The contact-cement theory is based on a theory of elasticity solution for the elastic deformation of two elastic spheres that are cemented at their contact. The properties of the cement material can be different from those of the grains. In the heart of the solution is contact stress distribution at the grain contact.

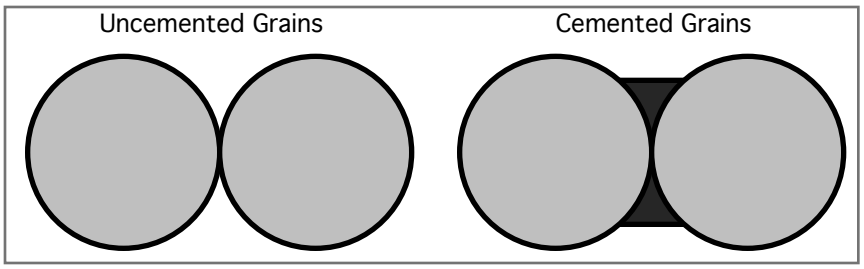

The contact stress distribution is completely different form that of two uncemented grains (the Hertz-Mindlin solution). Moreover, the contact stress distribution depends on the relative stiffness of the cement and the grains.

This property has important implication for grain disintegration under stress and sanding. It is also important for designing materials for reinforcing sand (e.g., artificial wellbore filter, pavements, protective walls).

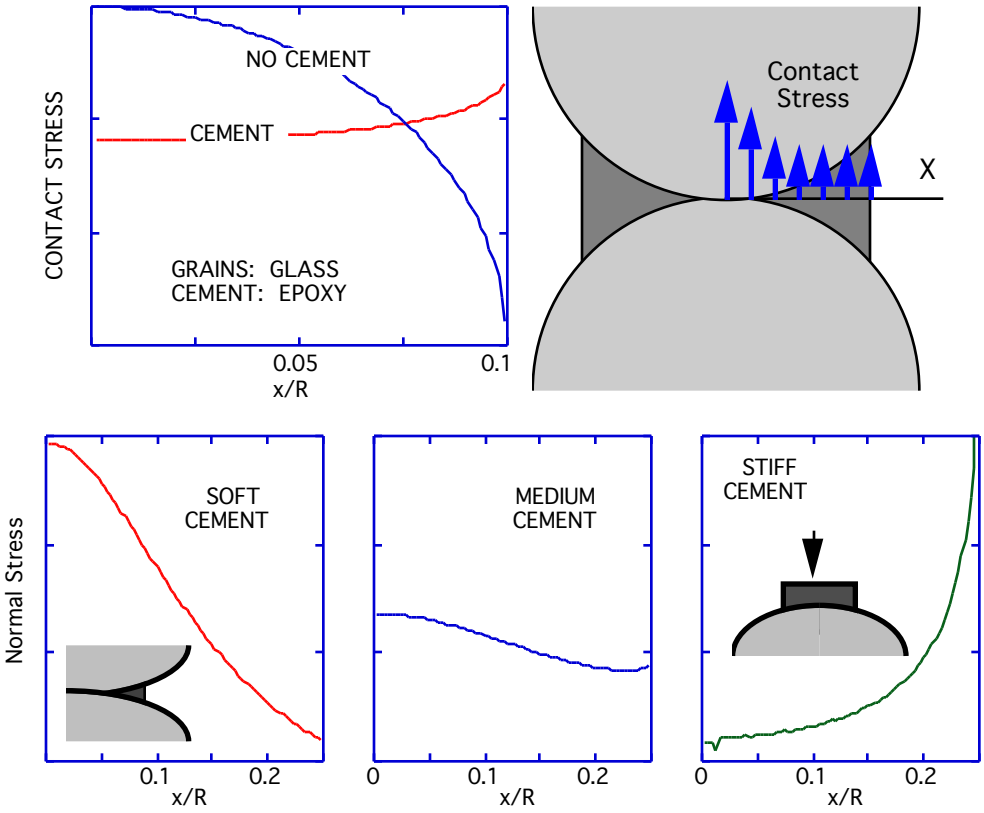

Photo-elastic experiment confirms the theoretical stress distribution results.

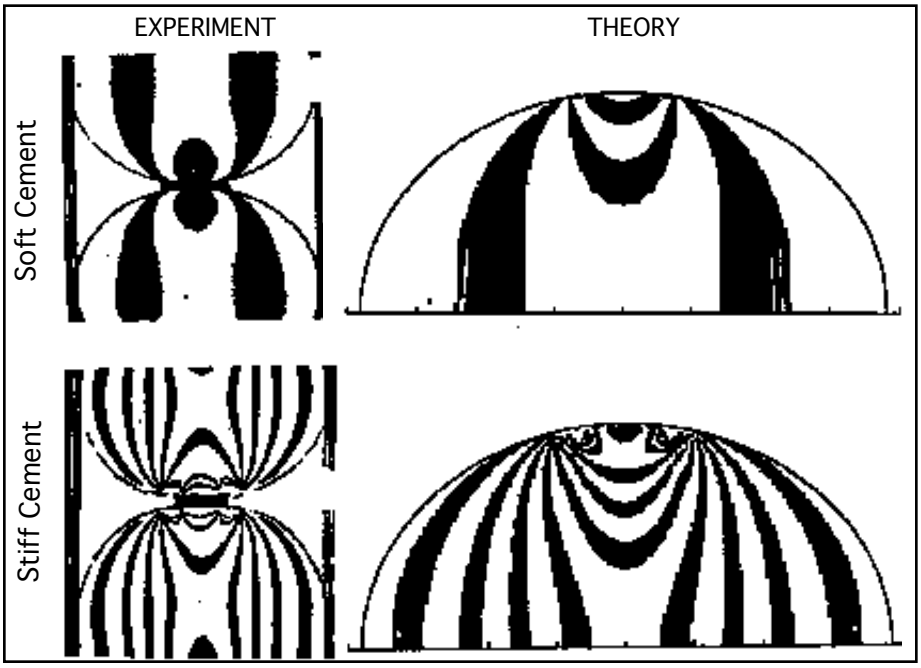

An experiment on epoxy-cemented glass bead compaction shows that even small amounts of contact cement prevent grain disintegration. This result has an important implication for strength and sanding potential.

The theoretical contact stress prediction explains the observed phenomenon: even small epoxy concentration (5% pore space saturation) results in evenly distributed contact stresses whereas the contact stress between the uncemented grains has a concentration at the center of contact.

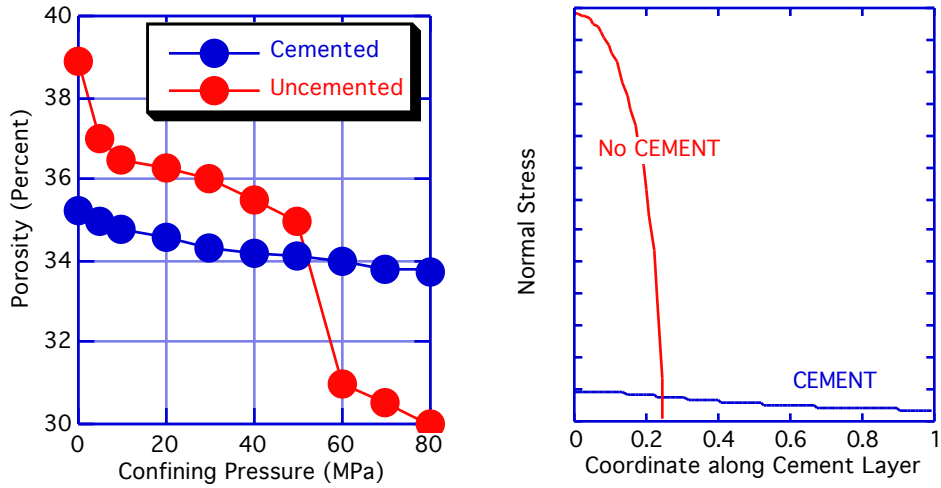

The contact cement theory has been confirmed by controlled-experiment data on glass beads. It also works for natural sediments (see above and below).

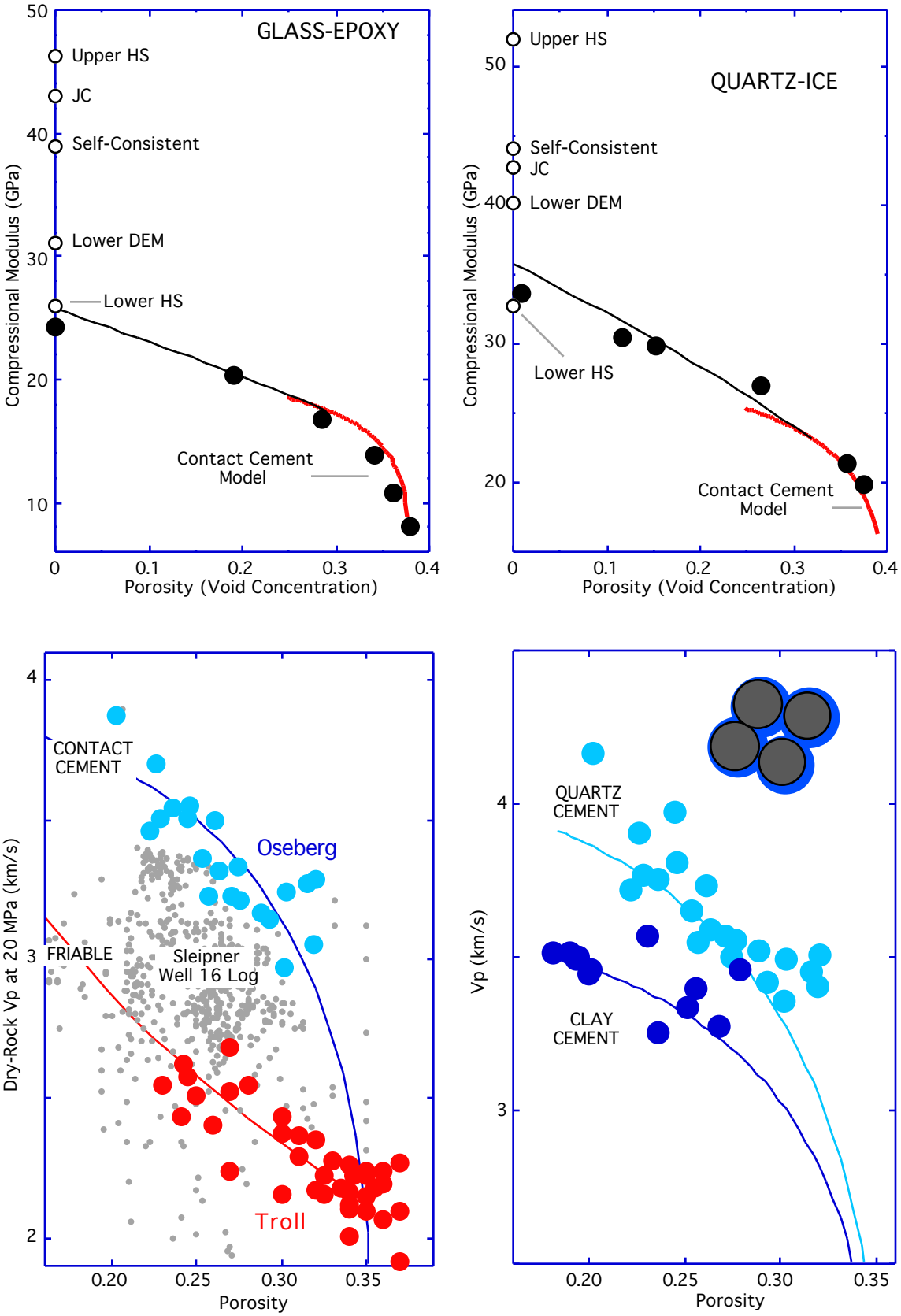
GLASS-EPOXY
Upper HS
JC
Self-Consistent
Lower DEM
Lower HS
Contact Cement Model
Compressional Modulus (GPa)
Porosity (Void Concentration)
QUARTZ-ICE
Upper HS
Self-Consistent
JC
Lower DEM
Lower HS
Contact Cement Model
Compressional Modulus (GPa)
Porosity (Void Concentration)
CONTACT CEMENT
Oseberg
FRIABLE
Sleipner Well 16 Log
Troll
Dry-Rock Vp at 20 MPa (km/s)
Porosity
QUARTZ CEMENT
CLAY CEMENT
Vp (km/s)
Porosity

9. Friable Sand Theory

The friable-sand (unconsolidated) model is based on the contact theory for uncemented grains. The two end-point are connected in the modulus-porosity plane: one at zero porosity that has the elastic moduli of the solid phase and the other at the critical porosity that has the elastic moduli of a random dense pack of identical elastic particles. The connecting curve is the lower-bound Hashin-Shtrikman curve.

The effect of saturation is calculated using Gassmann's equation.

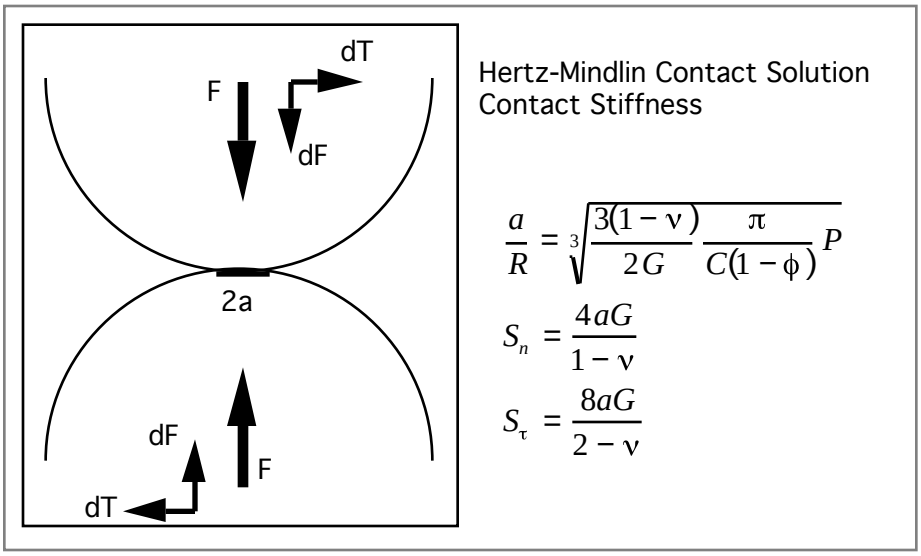

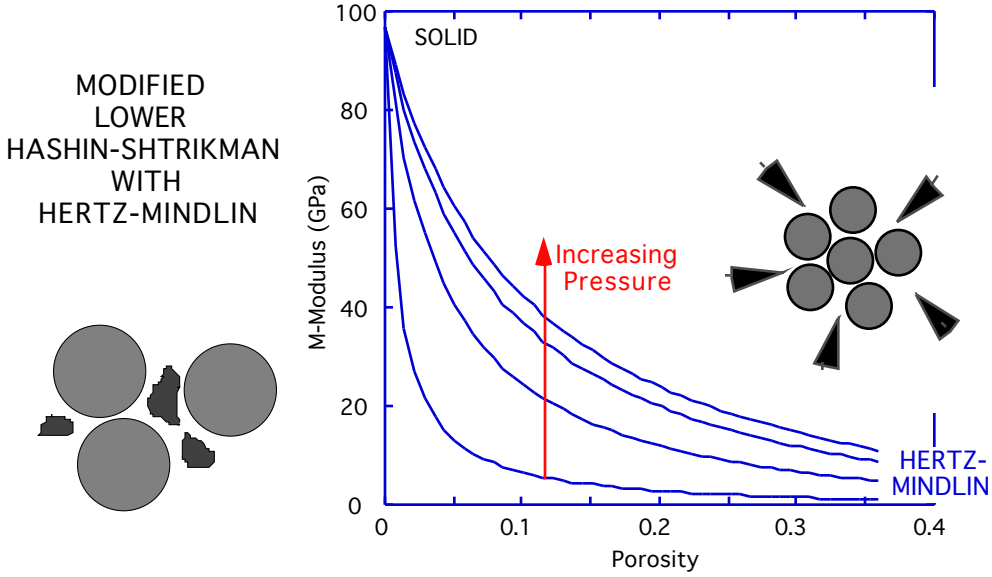

This model has confirmation in experimental data as well as in well-log data (see below).

This velocity-porosity transform can be applied, for example in soft sands to infer porosity from velocity in a cased hole (see example below).

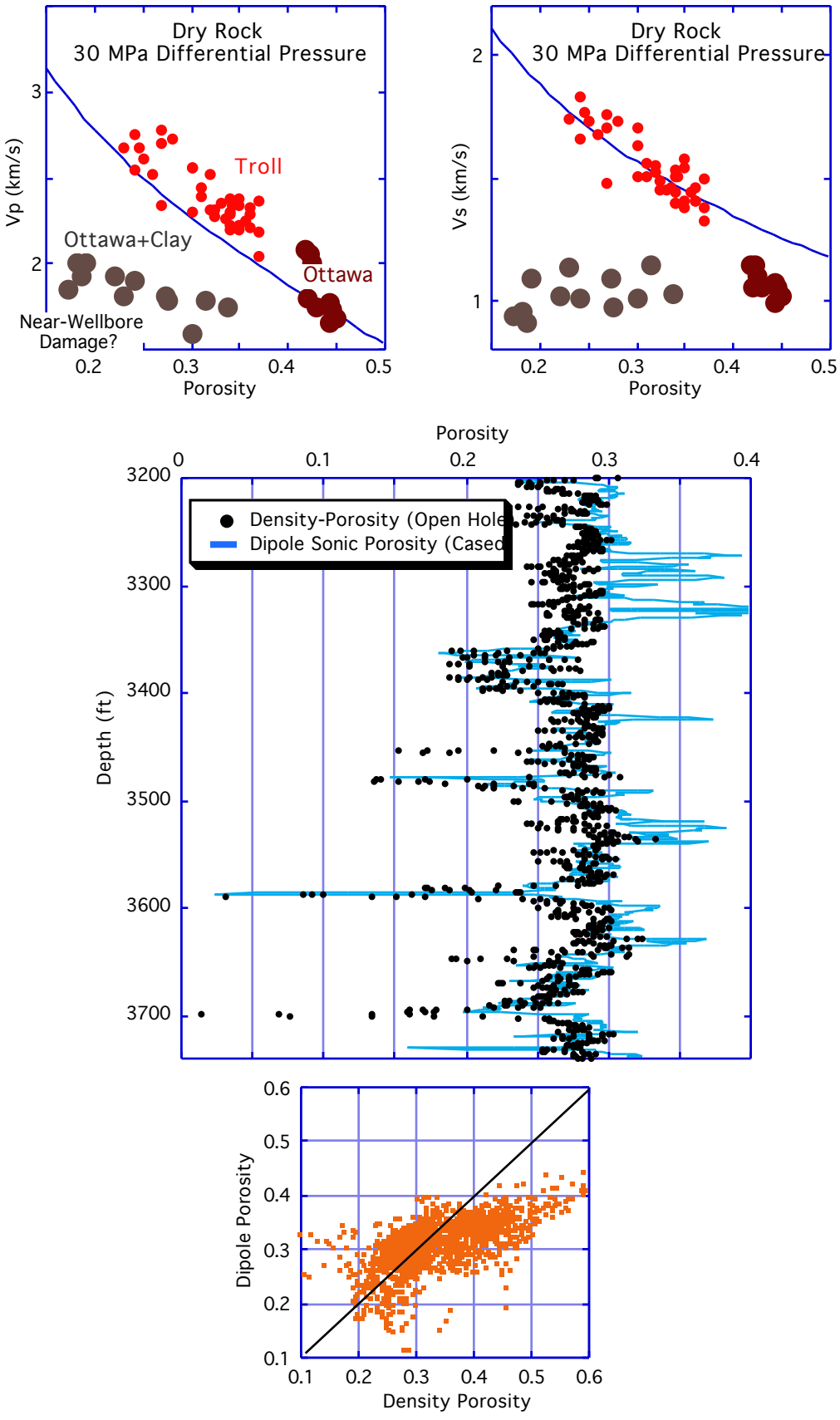
Dry Rock
30 MPa Differential Pressure
Vp (km/s)
Troll
Ottawa+Clay
Ottawa
Near-Wellbore
Damage?
Porosity
Dry Rock
30 MPa Differential Pressure
Vs (km/s)
Porosity
Porosity
Density-Porosity (Open Hole)
Dipole Sonic Porosity (Cased)
Depth (ft)
Dipole Porosity
Density Porosity

10. Formal Model Description

The initial building point for effective medium models that describe high-porosity sandstones should be unconsolidated well-sorted sand, as proposed by the critical porosity concept. In mathematical modeling, such sand is approximated by a dense pack of identical elastic spheres.

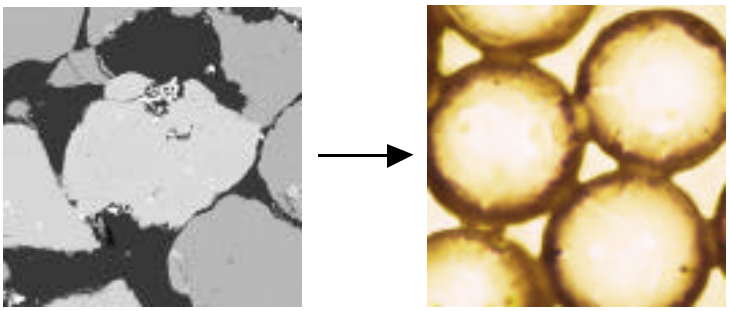

Approximating sand by a sphere pack (microphotographs of well-sorted sand, left, and a glass-bead pack, right).

The ***contact-cement model*** (Dvorkin and Nur, 1996) assumes that porosity reduces from the initial critical porosity value due to the uniform deposition of cement layers on the surface of the grains.

This cement may be diagenetic quartz, calcite, or reactive clay (such as illite). The diagenetic cement dramatically increases the stiffness of the sand by reinforcing the grain contacts. The mathematical model is based on a rigorous contact-problem solution by Dvorkin et al. (1994).

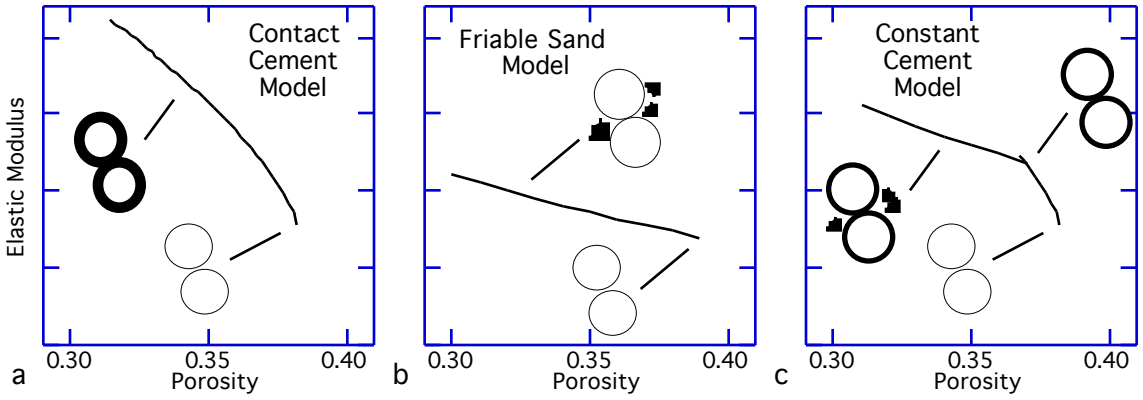

Schematic depiction of three effective-medium models for high-porosity sandstones and corresponding diagenetic transformations.

In this model, the effective bulk (K_{dry}) and shear (G_{dry}) moduli of dry rock are:

$$K_{dry} = n(1-\phi_c)M_c S_n / 6,\ G_{dry} = 3K_{dry}/5 + 3n(1-\phi_c)G_c S_\tau / 20, \qquad (3.10.1)$$

where ϕ_c is critical porosity; K_s and G_s are the bulk and shear moduli of the grain material, respectively; K_c and G_c are the bulk and shear moduli of the cement material, respectively;

$M_c = K_c + 4G_c/3$ is the compressional modulus of the cement; and n is the coordination number -- average number of contacts per grain (8-9). S_n and S_τ are:

$$S_n = A_n(\Lambda_n)\alpha^2 + B_n(\Lambda_n)\alpha + C_n(\Lambda_n),\ A_n(\Lambda_n) = -0.024153\ \ \Lambda_n^{-1.3646},$$
$$B_n(\Lambda_n) = 0.20405\ \ \Lambda_n^{-0.89008},\ C_n(\Lambda_n) = 0.00024649\ \ \Lambda_n^{-1.9864};$$
$$S_\tau = A_\tau(\Lambda_\tau, \nu_s)\alpha^2 + B_\tau(\Lambda_\tau, \nu_s)\alpha + C_\tau(\Lambda_\tau, \nu_s),$$
$$A_\tau(\Lambda_\tau, \nu_s) = -10^{-2}\ \ (2.26\nu_s^2 + 2.07\nu_s + 2.3)\ \ \Lambda_\tau^{0.079\nu_s^2 + 0.1754\nu_s - 1.342},$$
$$B_\tau(\Lambda_\tau, \nu_s) = (0.0573\nu_s^2 + 0.0937\nu_s + 0.202)\ \ \Lambda_\tau^{0.0274\nu_s^2 + 0.0529\nu_s - 0.8765},$$
$$C_\tau(\Lambda_\tau, \nu_s) = 10^{-4}\ \ (9.654\nu_s^2 + 4.945\nu_s + 3.1)\ \ \Lambda_\tau^{0.01867\nu_s^2 + 0.4011\nu_s - 1.8186};$$
$$\Lambda_n = 2G_c(1-\nu_s)(1-\nu_c)/[\pi G_s(1-2\nu_c)],\ \Lambda_\tau = G_c/(\pi G_s);$$
$$\alpha = [(2/3)(\phi_c - \phi)/(1-\phi_c)]^{0.5};$$
$$\nu_c = 0.5(K_c/G_c - 2/3)/(K_c/G_c + 1/3);$$
$$\nu_s = 0.5(K_s/G_s - 2/3)/(K_s/G_s + 1/3).$$

The contact cement theory allows one to accurately model the velocity in fast high-porosity sands. One may find that the contact-cement model is appropriate for describing sands in high-energy depositional environment where the grains are well-sorted and not covered by organic matter.

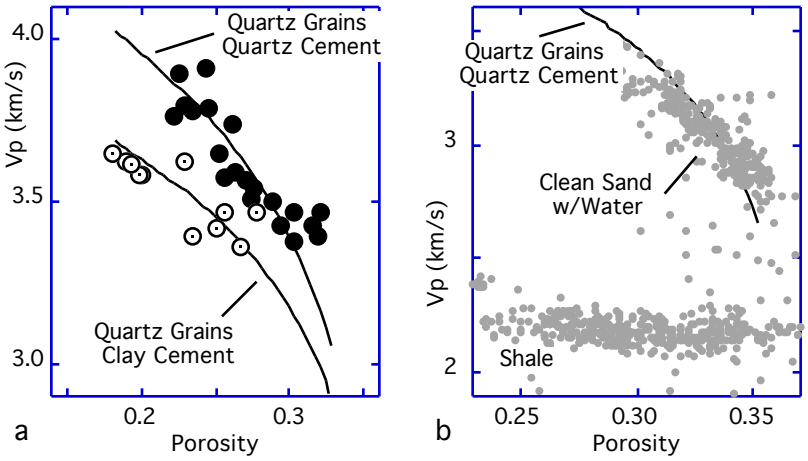

P-wave velocity versus porosity. a. Water-saturated-rock data based on laboratory measurements of fast high-porosity North Sea sandstones by Strandenes (1991). Solid circles are for very clean samples. Open circles are for samples with some clay. The curves are from the contact cement model for pure quartz grains with quartz and clay cement. b. Well-log data. The clean sand interval is saturated with water. The curve is from the contact cement theory for pure quartz grains with quartz cement.

The ***friable sand model*** (Dvorkin and Nur, 1996) assumes that porosity reduces from the initial critical porosity value due to the deposition of the solid matter away from the grain contacts. Such a diagenetic process of porosity reduction may correspond to deteriorating grain sorting. This non-contact additional solid matter weakly affects the stiffness of the rock.

The theoretical effective-medium model connects two end-points in the elastic-modulus-porosity plane. One end point is at critical porosity. The elastic moduli of the dry rock at that point are assumed to be the same as of an elastic sphere pack subject to confining pressure. These moduli are given by the Hertz-Mindlin (Mindlin, 1949) theory:

$$K_{HM} = \left[\frac{n^2(1-\phi_c)^2 G^2}{18\pi^2(1-\nu)^2} P\right]^{\frac{1}{3}},$$
$$G_{HM} = \frac{5-4\nu}{5(2-\nu)}\left[\frac{3n^2(1-\phi_c)^2 G^2}{2\pi^2(1-\nu)^2} P\right]^{\frac{1}{3}}; \qquad (3.10.2)$$

where K_{HM} and G_{HM} are the bulk and shear moduli at critical porosity ϕ_c, respectively; P is the differential pressure; K, G, and ν are the bulk and shear moduli of the solid phase, and its Poisson's ratio, respectively; and n is the coordination number.

The other end-point is at zero porosity and has the bulk (K) and shear (G) moduli of the pure solid phase. These two points in the porosity-moduli plane are connected with the curves that have the algebraic expressions of the lower Hashin-Shtrikman (1963) bound (bulk and shear moduli) for the mixture of two components: the pure solid phase and the phase that is the sphere pack. The reasoning is that in unconsolidated sediment, the softest component (the sphere pack) envelopes the stiffest component (the solid) in the Hashin-Shtrikman fashion.

At porosity ϕ the concentration of the pure solid phase (added to the sphere pack to decrease porosity) in the rock is $1-\phi/\phi_c$ and that of the sphere-pack phase is ϕ/ϕ_c. Then the bulk (K_{Dry}) and shear (G_{Dry}) moduli of the dry frame are:

$$K_{Dry} = \left[\frac{\phi/\phi_c}{K_{HM}+\frac{4}{3}G_{HM}} + \frac{1-\phi/\phi_c}{K+\frac{4}{3}G_{HM}}\right]^{-1} - \frac{4}{3}G_{HM},$$
$$G_{Dry} = \left[\frac{\phi/\phi_c}{G_{HM}+z} + \frac{1-\phi/\phi_c}{G+z}\right]^{-1} - z,\ z = \frac{G_{HM}}{6}\left(\frac{9K_{HM}+8G_{HM}}{K_{HM}+2G_{HM}}\right). \qquad (3.10.3)$$

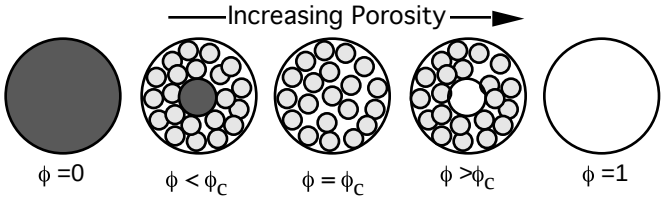

Hashin-Shtrikman arrangements of sphere pack, solid, and void.

The friable sand model allows one to accurately predict velocity in soft high-porosity sands. This model is appropriate for describing sands where contact cement deposition was inhibited by organic matter deposited on the grain surface.

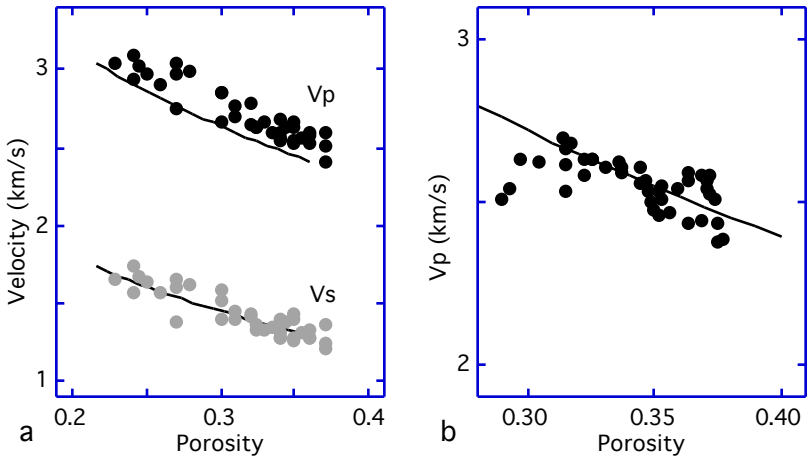

Velocity versus porosity. a. Water-saturated-rock data based on laboratory measurements of soft high-porosity North Sea sandstones by Blangy (1992). b. Well-log data (Avseth et al., 1998) for oil-saturated pay zone. The curves are from the friable sand model.

The ***constant-cement model*** (Avseth et al., 1998) assumes that the initial porosity reduction from critical porosity is due to the contact cement deposition. At some high porosity, this diagenetic process stops and after that porosity reduces due to the deposition of the solid phase away from the grain contacts as in the friable sand model (Figure 1.8c). This model is mathematically analogous to the friable sand model except that the high-porosity end point bulk and shear moduli (K_b and G_b, respectively) are calculated at some "cemented" porosity ϕ_b from the contact-cement model. Then the dry-rock bulk and shear moduli are:

$$K_{dry} = \left(\frac{\phi / \phi_b}{K_b + 4G_b/3} + \frac{1-\phi/\phi_b}{K_s + 4G_b/3}\right)^{-1} - 4G_b/3,$$
$$G_{dry} = \left(\frac{\phi / \phi_b}{G_b + z} + \frac{1-\phi/\phi_b}{G_s + z}\right)^{-1} - z, \qquad (3.10.4)$$
$$z = \frac{G_b}{6}\frac{9K_b + 8G_b}{K_b + 2G_b}.$$

An example of applying this model to well-log data is given below.

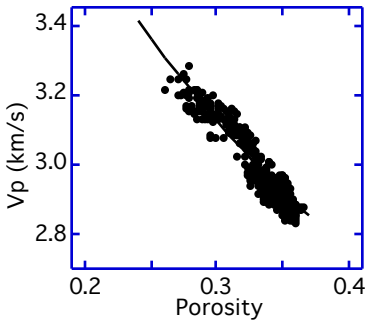

Velocity versus porosity. Well-log data (Avseth et al., 1998) for oil-saturated pay zone. The curve is from the constant cement model.

Model for unconsolidated marine sediment. This model (Dvorkin et al., 1999) is analogous to the friable sand model but covers the porosity range above critical porosity. One end point is the critical porosity where the elastic moduli of the sphere pack are given by Equations (3.10.2). To arrive at higher porosity, we add empty voids to the sphere pack. In this case the voids are placed inside the pack in the Hashin-Shtrikman fashion. Now the pack is the stiffest component, so we have to use the upper Hashin-Shtrikman limit.

At porosity $\phi > \phi_c$, the concentration of the void phase is $(\phi - \phi_c)/(1-\phi_c)$ and that of the sphere-pack phase is $(1-\phi)/(1-\phi_c)$. Then the effective dry-rock frame bulk and shear moduli are:

$$K_{Dry} = \left[\frac{(1-\phi)/(1-\phi_c)}{K_{HM} + \frac{4}{3}G_{HM}} + \frac{(\phi-\phi_c)/(1-\phi_c)}{\frac{4}{3}G_{HM}}\right]^{-1} - \frac{4}{3}G_{HM},$$

$$G_{Dry} = \left[\frac{(1-\phi)/(1-\phi_c)}{G_{HM} + z} + \frac{(\phi-\phi_c)/(1-\phi_c)}{z}\right]^{-1} - z, \qquad (3.10.5)$$

$$z = \frac{G_{HM}}{6}\left(\frac{9K_{HM} + 8G_{HM}}{K_{HM} + 2G_{HM}}\right).$$

The saturated-rock elastic moduli can be calculated using Gassmann's (1951) equation.

An example of applying this model to log data is given below. A good agreement between the model and the data is apparent. At the same time, the often used suspension model fails to correctly mimic the data.

This model's departure from the data increases with depth which is due to the effect of confining pressure that adds stiffness to the dry frame of the sediment thus making the suspension model inadequate.

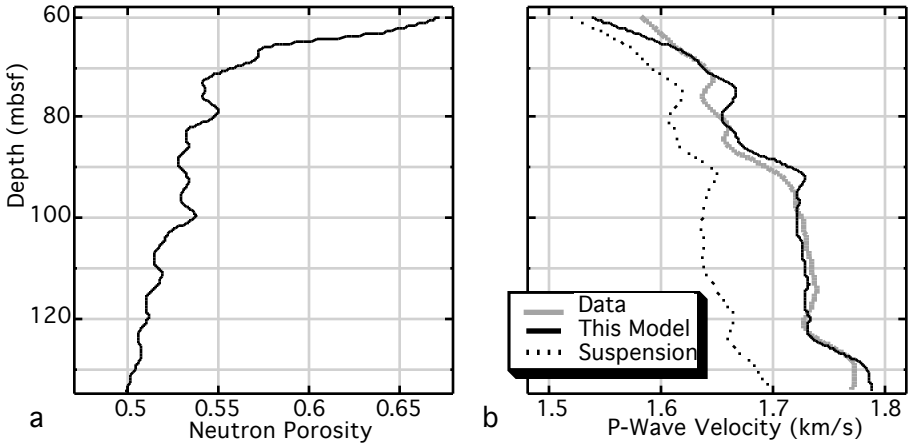

DSDP Well 974. a. Neutron porosity versus depth. b. Velocity versus depth: data, our model, and suspension model. All curves are smoothed.

The ***critical porosity and critical concentration concepts*** allow the geophysicist to better understand the diversity of well log and core elastic data. Effective-medium models built on the basis of the critical porosity concept can accurately model data.

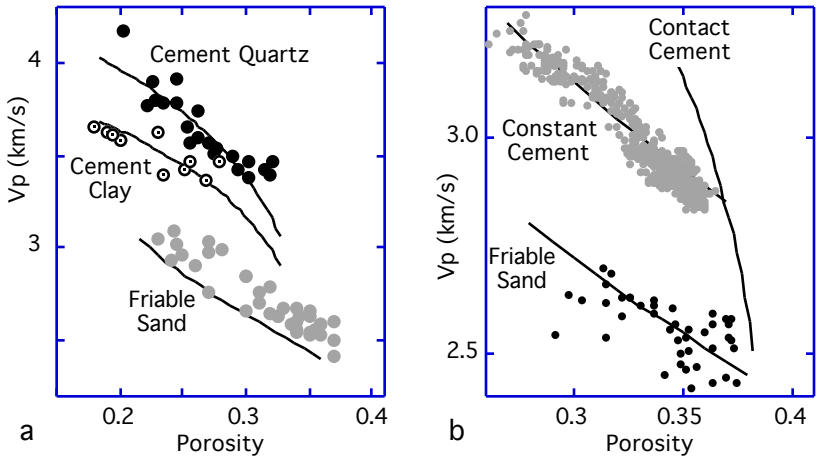

Velocity versus porosity. Theoretical curves superimposed on data allow one to identify the rock type.

By superimposing theoretical model curves on velocity-porosity and elastic-moduli-porosity crossplots, one may mathematically ***diagnose*** rock, i.e., determine the texture of the sediment (e.g., contact-cemented versus friable).